





RESEARCH ARTICLE | JUNE 05 2023

## Objective molecular dynamics investigation of dissociation and recombination kinetics in high-temperature nitrogen



Gunjan Pahlani  ; Erik Torres ; Thomas Schwartzentruber; Richard D. James 



*Physics of Fluids* 35, 067111 (2023)

<https://doi.org/10.1063/5.0150492>

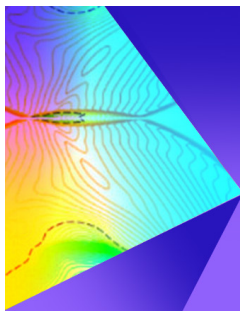


View  
Online



Export  
Citation

CrossMark



## Physics of Fluids

### Special Topic: Shock Waves

Submit Today!

# Objective molecular dynamics investigation of dissociation and recombination kinetics in high-temperature nitrogen

Cite as: Phys. Fluids **35**, 067111 (2023); doi: [10.1063/5.0150492](https://doi.org/10.1063/5.0150492)

Submitted: 14 March 2023 · Accepted: 7 May 2023 ·

Published Online: 5 June 2023



View Online



Export Citation



CrossMark

Gunjan Pahlani,<sup>a)</sup>  Erik Torres,<sup>b)</sup>  Thomas Schwartzentruber,<sup>c)</sup> and Richard D. James<sup>d)</sup> 

## AFFILIATIONS

Department of Aerospace Engineering and Mechanics, University of Minnesota, Minneapolis, Minnesota 55455, USA

<sup>a)</sup> Author to whom correspondence should be addressed: [pahla005@umn.edu](mailto:pahla005@umn.edu)

<sup>b)</sup> Electronic mail: [etorres@umn.edu](mailto:etorres@umn.edu)

<sup>c)</sup> Electronic mail: [schwart@umn.edu](mailto:schwart@umn.edu). URL: <https://sites.google.com/view/cgdl-schwartzentruber/home>

<sup>d)</sup> Electronic mail: [james@umn.edu](mailto:james@umn.edu). URL: <https://dept.aem.umn.edu/people/faculty/james/research/home.html>

## ABSTRACT

In this study, we propose the use of the novel approach of objective molecular dynamics (OMD) simulating far-from-equilibrium gas dynamics problems with chemical reactions. The OMD method has an exact relation to models in continuum mechanics and can be used to improve those models. We provide a detailed molecular dynamics investigation of chemically reacting nitrogen gas in a space-homogeneous adiabatic reactor. The analysis is based on a first-principles derived reactive ReaxFF potential energy surface, which captures the relevant processes of rovibrational relaxation, dissociation, and exchange as well as recombination in a gas evolving under non-equilibrium conditions. We examine the evolution of the internal mode population distribution of all the molecules as well as the rovibrational probability distribution of the pre-collision dissociating and post-collision recombined  $N_2$  molecules to investigate the microscopic selectivity of various reactive processes. Subsequently, we make comparisons with results obtained by means of an alternative modeling approach called direct molecular simulation. The current work illustrates the application of the method of OMD to study the compression and expansion kinetics of dissociation-recombination nitrogen mixture relevant to normal shock wave and nozzle expansion.

Published under an exclusive license by AIP Publishing. <https://doi.org/10.1063/5.0150492>

## I. INTRODUCTION

Hypersonic flows characterized by high Mach numbers typically involve shock waves and rapid expansions, which can cause the gas to become vibrationally excited and chemically reacting. The strong thermochemical non-equilibrium effects are present in the gas when the timescales of flow and internal energy transfer and chemistry are of similar orders of magnitude. Computational fluid dynamics (CFD) models the flow as a continuum and relies on various traditional transport, energy exchange, and chemistry models, which, though accurate in the near-equilibrium regime, are known to break down under strong non-equilibrium conditions. This breakdown can either be due to non-linear transport<sup>1–4</sup> or strong thermo-chemical non-equilibrium.<sup>5–7</sup>

An alternative set of the modeling approaches is based on particle-level methods where individual molecules and atoms are tracked either statistically (DSMC)<sup>8,9</sup> or deterministically (MD).<sup>10,11</sup> The DSMC method has been shown to simulate the Boltzmann transport equation (BTE), which defines the evolution of the velocity and

internal energy distribution functions. It has had success in describing dilute flows over wide regimes and is one of the most successful particle simulation methods for rarefied gaseous flows. However, DSMC requires collision cross section models as input for inelastic and reacting collisions. The traditional collision cross-sectional models used as input to DSMC require many parameters, many of which are still uncertain.

The desire to remove these uncertainties and avoid empiricism led to the development of the direct molecular simulation (DMS) method.<sup>12,13</sup> DMS integrates exact classical trajectory calculation on an *ab initio* potential energy surface (PES) for each binary collision within a DSMC simulation and, thus, apart from the dilute gas assumption (which allows decoupling of free molecular motion from collisions over small enough timescales), the solution is based on the sole input of PESs. Hence, the method can be understood as a method of “Accelerated MD” for modeling of dilute gases. However, the current implementation of DMS cannot completely describe reacting

flows since three-body interactions are not simulated. In classical dynamics, the third body carries away enough excess energy from the interacting two-atom system (in the form of the third body's kinetic energy) so that they can stay bounded at an internal energy inside the diatomic potential well. Otherwise they approach each other in the center of mass frame only to separate again without forming a stable molecule. Additionally, momentum should be conserved in the collision. Therefore, this needs modeling of three-body collisions, which is still a subject of active research.<sup>14</sup> Thus, the recombination reaction has not been investigated at the same level of detail using *ab initio* particle methods under non-equilibrium conditions, as processes of dissociation and exchange have. Consideration of all these processes is important to predict the correct thermochemical gas state around a hypersonic vehicle, which directly influences heat flux to the surface and gas-surface reactions.

In this paper, we focus on studying all the relevant electronic ground-state processes in nitrogen: rovibrational relaxation, dissociation, exchange as well as recombination using the pure deterministic method of molecular dynamics. Unlike DMS, our method captures three and many-body collisions and, hence, automatically incorporates recombination as well. We are able to do this because of particular features of the method of objective molecular dynamics (OMD) explained below.

Traditional molecular dynamics (MD) of spatially homogeneous systems, where Newton's equations of motion are solved for every atom, typically replicates an adiabatic reactor where the total energy of the system is conserved. MD can also be used to replicate an isothermal reactor where the system is assumed to be temperature controlled by a heat bath,<sup>11</sup> though these approaches typically introduce artificial forces on atoms, which guarantee that a certain distribution of statistical mechanics is being modeled and, therefore, are not suitable to the accurate modeling of chemical reactions. Similarly, DMS can generate adiabatic/isothermal conditions. Most prior work along these lines has focused on non-equilibrium relaxation of a dissociating gas where the gas is initialized in thermo-chemical non-equilibrium.<sup>15–17</sup>

In this study, we introduce the method of objective molecular dynamics (OMD), which extends the capability of MD to systems beyond adiabatic and isothermal reactors for analyzing the non-equilibrium physics of gases. In OMD one simulates flow fields having a macroscopic form  $\mathbf{v} = \mathbf{A}(\mathbf{I} + t\mathbf{A})^{-1}\mathbf{x}$ , where  $\mathbf{I}$  is an Identity matrix,  $t$  is time, and  $\mathbf{A}$  is an arbitrary assigned constant  $3 \times 3$  matrix.<sup>18–20</sup> An advantage of these flows is their compatibility with fluid dynamics, i.e., the velocity field  $\mathbf{v}(\mathbf{x}, t) = \mathbf{A}(\mathbf{I} + t\mathbf{A})^{-1}\mathbf{x}$  is an exact solution of the macroscopic momentum conservation equation of fluid dynamics for many well-accepted transport constitutive models. This allows us to bridge the gap between molecular and continuum theory by making connections and formulating better transport and chemistry models from first principles, which can improve the predictions of higher scale modeling. One such effort is to develop a non-classical constitutive model for OMD flows of dilute mono-atomic gases, which improve Navier–Stokes prediction under strong gradients.<sup>1,2</sup> Also, the statistical distribution of velocities in an OMD simulation is known to have the form  $f(t, \mathbf{x}, \mathbf{v}) = g(t, \mathbf{v} - \mathbf{A}(\mathbf{I} + t\mathbf{A})^{-1}\mathbf{x})$ . Substitution of the formula  $f(t, \mathbf{x}, \mathbf{v}) = g(t, \mathbf{v} - \mathbf{A}(\mathbf{I} + t\mathbf{A})^{-1}\mathbf{x})$  into the Boltzmann equation gives an exact reduction to an evolution law for  $g$ . In other words, the statistics of the MD solutions in OMD are exactly consistent with the statistics of the Boltzmann equation. (However, OMD is not restricted

to rarefied gases: It can be applied to solids<sup>21</sup> and also nanostructures.<sup>22</sup>) The solution of this reduced Boltzmann equation can give interesting insight into far-from-equilibrium statistical mechanics.<sup>23,24</sup>

Objective molecular dynamics (OMD) is a generalization of traditional molecular dynamics with periodic boundary conditions to non-equilibrium systems. OMD is symmetry-adapted MD, which is based on fundamental invariances (invariance under orthogonal transformations, translations, and permutations) of the underlying Born–Oppenheimer potential energy surface and the special structure of MD equations. These symmetries are represented by isometry groups, i.e., groups of orthogonal transformations and translations. In OMD, we define a finite set of “simulated atoms,” which are denoted by  $\mathbf{y}_k(t)$ ,  $k = 1, \dots, M$ . The value of  $M > 1$  and the initial conditions for the simulated atoms are assignable. All the other atoms (typically infinite) of the system (the “non-simulated atoms”) are obtained by applying isometry groups to the set of simulated atoms. For fluid flows considered here, the relevant isometry group is the group of time-dependent pure translations. This results in the trajectory of non-simulated atoms given as a function of simulated atoms by the formula,

$$\begin{aligned} \mathbf{y}_{(\nu,k)}(t) &= \mathbf{y}_k(t) + (\mathbf{I} + t\mathbf{A})(\nu_1\mathbf{e}_1 + \nu_2\mathbf{e}_2 + \nu_3\mathbf{e}_3), \\ \nu &= (\nu_1, \nu_2, \nu_3), \quad \nu_i \in \mathbb{Z}, \quad k = 1, \dots, M, \\ \mathbf{v}_{(\nu,k)}(t) &= \mathbf{v}_k(t) + \mathbf{A}(\nu_1\mathbf{e}_1 + \nu_2\mathbf{e}_2 + \nu_3\mathbf{e}_3), \end{aligned} \quad (1)$$

where the non-simulated atoms ( $\mathbf{y}_{\nu,k}$ ,  $\mathbf{v}_{\nu,k}$ ) are parameterized by triplet of integers  $\nu = (\nu_1, \nu_2, \nu_3)$  and  $\mathbf{e}_1$ ,  $\mathbf{e}_2$ , and  $\mathbf{e}_3$  are three linearly independent vectors. Thus, for every simulated atom  $\mathbf{y}_k(t)$  at time  $t$ , there exist infinitely many non-simulated atoms  $\mathbf{y}_{(\nu,k)}(t)$  whose positions are obtained by extending the position of simulated atoms using the instantaneous periodicity defined by the three vectors  $((\mathbf{I} + t\mathbf{A})\mathbf{e}_1, (\mathbf{I} + t\mathbf{A})\mathbf{e}_2, (\mathbf{I} + t\mathbf{A})\mathbf{e}_3)$ . The set of integers  $\nu = (\nu_1, \nu_2, \nu_3)$  defines the degree of this extension.

The  $3 \times 3$  matrix  $\mathbf{A}$  is also assignable and is the same  $\mathbf{A}$  as appears in the macroscopic velocity field  $\mathbf{v}(\mathbf{x}, t) = \mathbf{A}(\mathbf{I} + t\mathbf{A})^{-1}\mathbf{x}$ . The main theorem of OMD states that if the MD equations are only solved for simulated atoms, and all the other non-simulated atoms are simply obtained by formula (1) at every  $t$ ; then, all the atoms, simulated and non-simulated, satisfy the MD equations exactly for their forces. This theorem computationally simplifies the problem to a great extent since only finitely many atoms (simulated atoms) need to be simulated. The sensitivity of the behavior of system of dilute gas with respect to number of simulated atoms is investigated in our previous work.<sup>25</sup> If the number of simulated atoms is too small, then simulation may become non-physical. As a general rule, we try to maintain the size of fundamental domain of simulated atoms to be higher than the length scale of the system (mean free path of gas), which provides the minimum number of simulated atoms at a given density. For the computation of forces acting on simulated atoms from all other atoms (simulated and non-simulated atoms), one needs to also keep track of non-simulated atoms. Typically, since the simulated atoms quickly diffuse into the “sea” of non-simulated atoms, the atoms within the cutoff of a given simulated atom at a given time step consist of both simulated and non-simulated atoms. Hence, at each time step, we only need to calculate the positions of these atoms within the cutoff of each simulated atom, in order to calculate the force on that simulated atom. The theorem underlying OMD says that, if this procedure is followed,

then each non-simulated atom also satisfies exactly the equations of molecular dynamics for its forces. All the computational details of the method are provided in Refs. 21 and 25.

The primary potential of OMD (similar to MD) is that it is not limited to binary collisions. Thus, it provides a suitable machinery to study recombination and condensation, which require models in many statistical based methods developed for the dilute gas regime.

Our main goal in this work is to present an exhaustive treatment of chemically reacting nitrogen gas under strong non-equilibrium conditions using pure molecular dynamics. Before discussing simulation results, in Sec. II, we give a brief overview of the ReaxFF potential energy surface for nitrogen being used in this work. We then analyze the system in dissociation-dominated and recombination-dominated regimes in an adiabatic MD reactor ( $\mathbf{A} = \mathbf{0}$ ). This is investigated in Secs. III and IV. These regimes are characterized by conditions where the mole fraction of molecular nitrogen at  $t = 0$  is, respectively, higher, or lower than that of the true equilibrium state, respectively. We make comparison with DMS to assess the behavior of reactive ReaxFF potential used for this study.

Section V sets up an OMD reactor to study the kinetics of gas by making a special choice of the tensor  $\mathbf{A}$ .  $\mathbf{A}$  is tuned to access the regimes of opposing behavior, where energy in the translational mode (characterized by translational temperature  $T_t$ ) becomes greater/smaller than the energy stored in the rotational (temperature  $T_r$ ) and vibrational mode (temperature  $T_v$ ), as the gas evolves. These regimes are of interest in the modeling of shock wave and nozzle expansion, respectively. Under these conditions, we examine the relevant macroscopic fields and microscopic distributions to investigate the behavior of the gas in detail. Finally, the conclusions are contained in Sec. VI.

## II. POTENTIAL ENERGY SURFACE

Recent advances in computational resources have led to the use of quantum chemistry calculations for the development of potential energy surfaces for studying high-temperature chemistry.<sup>26,27</sup> The usage of these calculations has been limited to three and four-atom systems since it becomes prohibitively expensive to use these accurate *ab initio* methods for a larger system composed of a multitude of atoms and molecules. Therefore, DMS<sup>15,17,28</sup> and quasi-classical trajectory (QCT)<sup>14,29,30</sup> type calculations are focused on atom–diatom and diatom–diatom interactions. This development has made available the *ab initio* rate parameters for elementary collisional processes, which have also enabled the development of state-to-state (STS) modeling.<sup>31–34</sup> The four-atom-based *ab initio* potential hypersurface in its current form<sup>26</sup> is not suitable for molecular dynamics computation since there is no control over the possible number of atoms interacting at once in MD. For this reason, we use a ReaxFF potential energy surface fitted to a similar *ab initio* (4N) dataset generated using MS-CASPT2 calculations by Paukku *et al.*<sup>26</sup> ReaxFF is a bond-order-based potential that accounts for the contribution from various energies, which for binary collisions are given by<sup>35</sup>

$$E_{\text{ReaxFF}} = E_{\text{bond}} + E_{\text{over}} + E_{\text{under}} + E_{\text{val}} + E_{\text{pen}} + E_{\text{tors}} + E_{\text{conj}} \\ + E_{\text{vdWaaals}} + E_{\text{coulomb}},$$

where terms on the right hand side represent the contribution from bond energy  $E_{\text{bond}}$ , over-/undercoordination  $E_{\text{over}}$ ,  $E_{\text{under}}$ , valence angle energy  $E_{\text{val}}$ , torsion energy  $E_{\text{tors}}$ , conjugation effects  $E_{\text{conj}}$  and van der Waals interactions  $E_{\text{vdWaaals}}$  and Coulombic interactions

$E_{\text{coulomb}}$  between atom pairs. Each term is a function of bond-length-dependent bond order of the pair of atoms considered, which allows for a smooth transition from a non-bonded to bonded system with no discontinuities in energy or forces during reaction. The terms have specific functional forms with their respective fitting parameters. The reader is referred to Refs. 36 and 37 for complete details on the forms and fitting for nitrogen. Note that ReaxFF PES does not impose a limit on how many atoms may be interacting at any given time but the underlying electronic structure calculations were only valid for at most four interacting N atoms.

Figure 1 presents a curve fit for a ReaxFF two-body potential. The dataset is constructed by computing ReaxFF energies of an isolated system of two interacting nitrogen atoms by sequentially varying the distance ( $r$ ) between them. The aim of this least squares fitting is to compute quantized rovibrational energy levels based on the diatomic ReaxFF potential using a WKB approximation.<sup>30,38</sup> From the  $\text{N}_2$  diatomic potential, we find a total of 9194 rovibrational levels, of which 7025 are bound and 2169 of which are quasi-bound states. Bound states have internal energy lower than the dissociation energy  $D^0 = 9.7746$  eV, and quasi-bound states have internal energy higher than  $D^0$ . This spans a range of 288 and 54 rotational and vibrational states, respectively. These quantized levels are used later to construct an equilibrium Boltzmann distribution of rovibrational energy states of  $\text{N}_2$  at a given temperature for comparison with the instantaneous population distribution of an evolving gas under non-equilibrium conditions.

## III. COMPARISON OF MD WITH DMS UNDER DISSOCIATION DOMINATED ADIABATIC CONDITIONS

In this section, we perform adiabatic MD computations under high-temperature conditions and compare them with DMS.<sup>39</sup> This is equivalent to putting  $\mathbf{A} = \mathbf{0}$  under the framework of OMD, which corresponds to the NVE (constant energy) statistical ensemble. NVE stands for: particle number  $N$ , volume  $V$ , total energy  $E$  microcanonical ensemble. The DMS computation performed here uses the PES fit from Paukku *et al.*<sup>26</sup> The aim of the comparison is to consider DMS as a benchmark solution under this high-temperature dissociation-dominated regime and assess the performance of ReaxFF-based MD in analyzing non-equilibrium reacting flow. In this case, the system is initialized with pure molecular nitrogen with initial translational  $T_t$ ,

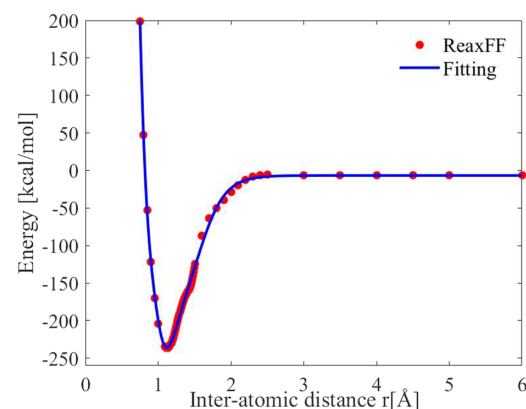
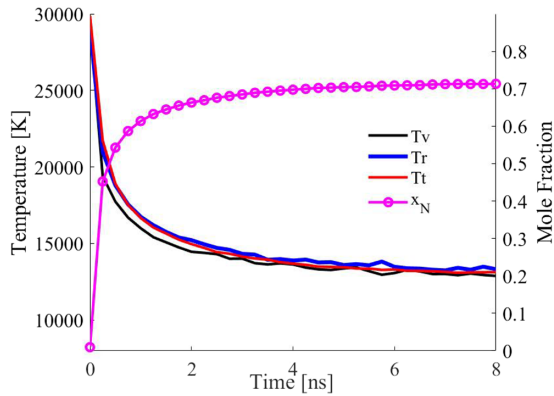


FIG. 1. Curve fitting of 2-body ReaxFF potential.



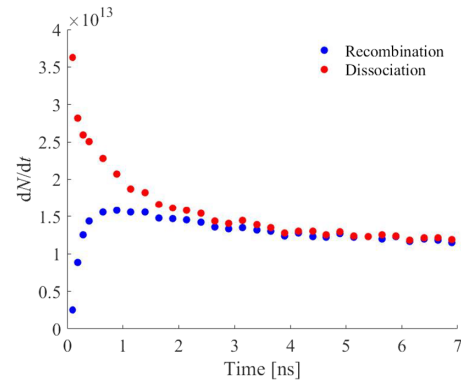
**FIG. 2.** Case 1: Adiabatic dissociation-dominated relaxation. Evolution of different temperatures and composition obtained by MD in dissociation dominated regime. Initial state:  $T_t = T_r = T_v = 30\,000\text{ K}$ ,  $\rho = 1.25\text{ kg/m}^3$ ,  $x_{N_2} = 1$ .

rotational  $T_r$ , and vibrational temperature  $T_v$  set to  $30\,000\text{ K}$  and density of  $\rho = 1.25\text{ kg/m}^3$  with  $100\,000$  simulated number of atoms. Note that the density (pressure) in these simulations was chosen to be high in order to force very high collision rates, which in turn make these MD simulations produce enough reaction events in a still reasonable amount of time steps. To post-process the phase-space trajectory, we store positions and velocities of all simulated atoms/molecules every few time steps and compute the internal energy states of molecules using the vibrational prioritized framework.<sup>40</sup> To extract the internal temperature from simulations, we use the definitions given by Panesi *et al.*<sup>31</sup> where the total internal energy of the system extracted from the simulation is equated to equivalent average energy based on the Maxwell–Boltzmann distribution for the rovibrational energy levels.

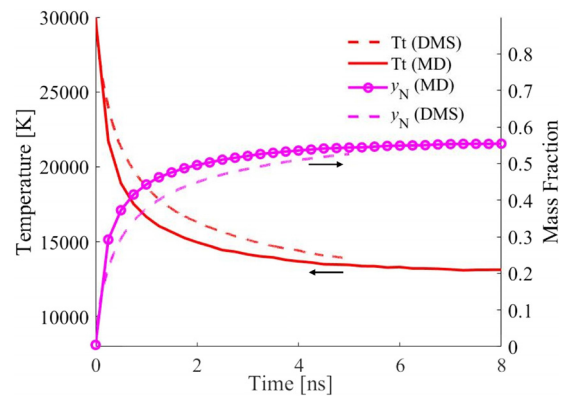
In this case, all the mode temperatures are initially high; therefore, the gas is already rovibrationally excited and the rate of dissociation is high from the start. Figure 2 shows the MD computed time evolution of different temperatures ( $T_t$ ,  $T_r$ ,  $T_v$ ) and mole fraction of atomic nitrogen ( $x_N$ ). As the system evolves, the mole fraction of atomic nitrogen increases due to dissociation. This process takes up energy from all the modes, which results in a decrease in the translational, rotational, and vibrational temperatures until the system reaches macroscopic equilibrium. In this high-temperature case, both internal energy modes relax together and this relaxation overlaps with the reactive processes, which leads to a strong coupling between the two.

Figure 3 examines the corresponding rate of dissociation (red circles) and recombination reactions (blue circles). As expected, it shows that dissociation dominates at an initial stage. As the system evolves, and temperature goes down, the rate of dissociation decreases and the rate of recombination increases. This is followed by a slow decrease in the magnitudes of both the forward and backward rates until they level off and reach a steady state.

Figures 4 and 5 compare the MD prediction with DMS. The reasonably close agreement between MD and DMS supports the suitability of ReaxFF potential for the study of nitrogen gas chemistry under non-equilibrium conditions. Note that the simulated conditions involve extremely high pressures. Even though the regime is dissociation dominated, it is clear that significant multibody events start



**FIG. 3.** Case 1: Adiabatic dissociation-dominated relaxation. Time evolution of number of dissociations and recombination events per unit time.



**FIG. 4.** Case 1: Adiabatic dissociation-dominated relaxation. Comparison of translational temperature  $T_t$  and mass fraction  $y_N$  with DMS (dashed lines).

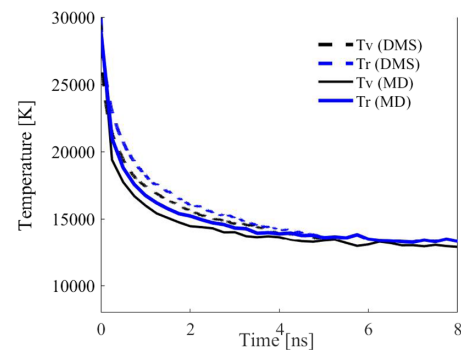


**FIG. 5.** Case 1: Adiabatic dissociation-dominated relaxation. Comparison of evolution of rotational and vibrational temperature with DMS (dashed lines).

happening in MD whereas in DMS, those interactions are not taken into account. The DMS code in its present state is only applicable to dilute gases dominated by 2-body interactions, and any higher-order interactions, such as the ones pre-requisite for recombination, are not

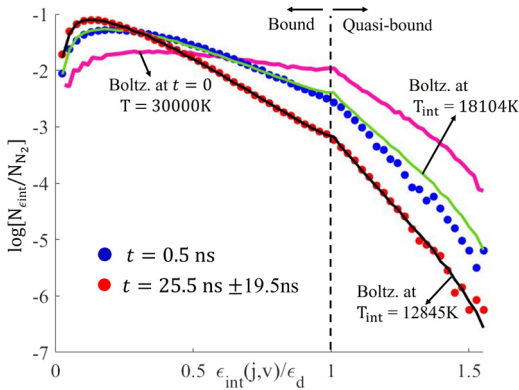


**FIG. 6.** Case 1: Adiabatic dissociation-dominated relaxation. Rovibrational energy populations (blue and red circles). Pink line depicts theoretical Boltzmann distribution at  $t = 0$ . Green and black lines: Boltzmann distribution at local internal temperature  $T_{int}$ . Initial state ( $t = 0$ ):  $T_t = T_r = T_v = 30\,000\text{ K}$ .

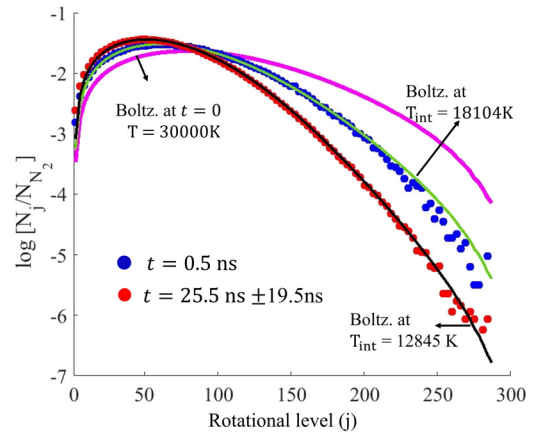


**FIG. 7.** Case 1: Adiabatic dissociation-dominated relaxation. Time evolution of rotational distribution functions (blue and red circles). Pink line depicts theoretical Boltzmann distribution at  $t = 0$ . Green and black lines: Boltzmann distribution at local internal temperature  $T_{int}$ . Initial state ( $t = 0$ ):  $T_t = T_r = T_v = 30\,000\text{ K}$ .

modeled. This can be one of the major reasons for the remaining differences seen in comparisons.

Next, we investigate population distribution functions at various time instants during the evolution to gain more microscopic insight into the gas dynamics. Figure 6 shows the internal (rotational + vibrational) energy population distributions where the vertical dashed line corresponds to the dissociation energy of  $N_2$  for the PES ( $D_0 = 9.77\text{ eV}$ ). The part toward the right of this line corresponds to quasi-bound states, and the part toward the left corresponds to bound states. Figures 7 and 8 show the distribution with respect to rotational and vibrational numbers, respectively. The system initiates at the imposed equilibrium distribution at  $T = 30\,000\text{ K}$  (solid pink line). Soon thereafter, at  $t = 0.5\text{ ns}$  (blue circles), the instantaneous distribution extracted from MD becomes depleted at higher internal energy levels due to the heavy preferential dissociation. This depletion with respect to a Boltzmann distribution at local internal temperature  $T_{int}$  (solid green line) significantly lowers the rate of dissociation as compared to a gas in local equilibrium as reported in earlier studies.<sup>15,17</sup> As time progresses the populations tend to the Boltzmann distribution as shown by time-averaged red circles in Figs. 6–8. The same feature is also evident from the evolution of the time-averaged dissociation probability density functions (PDFs) in Fig. 9. We define the dissociation probability density from a given internal energy [ $p^D(\epsilon_{int}(j, v))$ ]/rotational [ $p^D(j)$ ]/vibrational state [ $p^D(v)$ ] as the ratio of number of molecules dissociating from that internal energy/rotational/vibrational level to the total number of molecules, which dissociated in that time interval. This dissociation can be due to a collision with either another molecule or an atom. The probability is time-averaged over a time window to reduce statistical noise. The dissociation PDFs based on internal energy levels at all times have a strong peak near the dissociation limit  $D^0$  as shown in Fig. 9(a). Nevertheless, a non-negligible number of dissociations also originate from lower energy bound states. Initially, the contribution of these low-lying energy states is greater than high-lying states, as shown by blue circles at  $t = 0.5\text{ ns} \pm \Delta t_1$ . This is due to the increased availability of collision energy from translation ( $T_t \approx 18\,902\text{ K}$ ), which is often high enough to knock out atoms

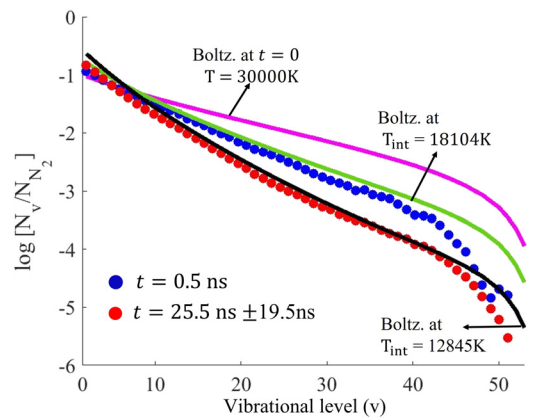


**FIG. 8.** Case 1: Adiabatic dissociation-dominated relaxation. Time evolution of vibrational population distribution functions (blue and red circles). Pink line depicts theoretical Boltzmann distribution at  $t = 0$ . Green and black lines: Boltzmann distribution at local internal temperature  $T_{int}$ . Initial state ( $t = 0$ ):  $T_t = T_r = T_v = 30\,000\text{ K}$ .

from molecular nitrogen bonded in low-energy states. This probability decreases as the system evolves, due to decrease in the translational temperature, which modifies the PDF shape, increasing the contribution of the quasi-bound states lying on the right side, as shown by the red circles at  $t = 2.5\text{ ns} \pm \Delta t_2$ . Note that time interval  $\Delta t_1 = 0.5\text{ ns}$  is chosen to be smaller than  $\Delta t_2 = 1.5\text{ ns}$  due to steep gradients observed at the initial stage. Similar characteristics of non-equilibrium dissociation PDFs are also reported in an earlier DMS study.<sup>15</sup>

The other plots in Fig. 9 show the pre-collision rotational and vibrational energy PDFs of dissociated reactants at two time instants, where the binning is based on rotational and vibrational quantum levels, respectively. It is apparent from the plots that molecules have a strong tendency to dissociate from higher vibrational levels. A similar assertion regarding vibrational bias has been made in Refs. 17 and 41. As time evolves and the translational and internal temperatures decrease, the bias shifts to the right of the dissociation PDF based on

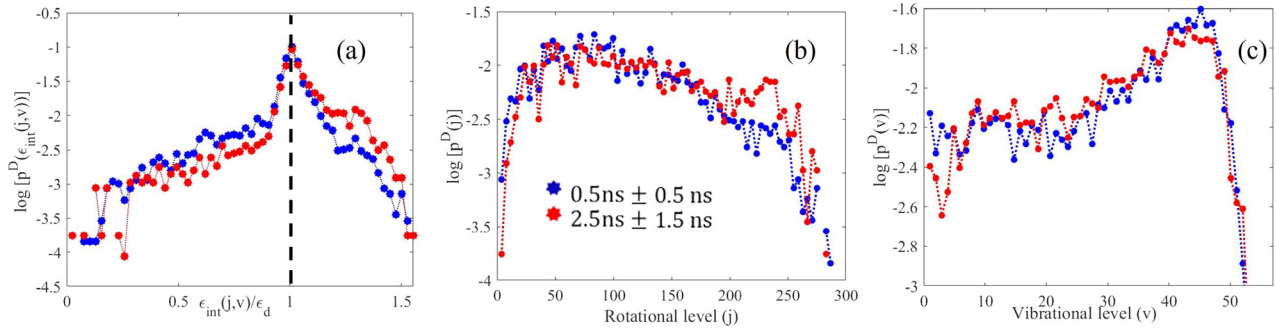


**FIG. 9.** Case 1: Adiabatic dissociation-dominated relaxation. Time-averaged evolution of dissociation probability density from a given (a) internal energy, (b) rotational, and (c) vibrational state, respectively. Blue and red circles depict density time averages over two distinct intervals (1 : [0, 1 ns]) and 2 : [1, 4 ns]), where  $(T_{t2} < T_{t1})$ .

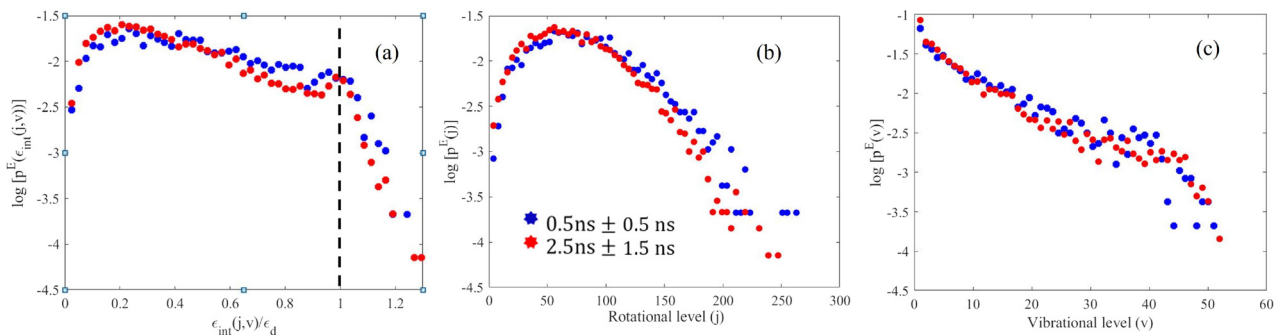


**FIG. 10.** Case 1: Adiabatic dissociation-dominated relaxation. Time-averaged evolution of post collision exchange probability density to a given (a) internal energy, (b) rotational, and (c) vibrational state, respectively. Blue and red circles depict density time averages over two distinct intervals (1 : [0, 1 ns]) and 2 : [1, 4 ns]), where  $(T_{t2} < T_{t1})$ .

rotational quantum number, increasing the contribution from higher rotational numbers [red circles which correspond to  $P^D(j)$  in Fig. 9(b)]. The shape of the dissociation probability density reflects the combined effects of continued dissociation with time, which leads to a scarcity of the molecules at certain levels of the vibrational and rotational manifolds, and an inherent favoring of dissociation processes for certain rovibrational levels  $(j, v)$ . Figure 10 shows the post-collision exchange probability density (red circles). The pre-collision molecules also display a similar probability density. In contrast to dissociation, the exchange PDF roughly follows the instant population distribution of all the molecules in the gas. This suggests that the exchange reaction has no microscopic bias toward any specific rovibrational state.

**IV. MD UNDER RECOMBINATION DOMINATED ADIABATIC CONDITIONS**

In this section, we focus on the recombination-dominated regime. That is, at the initial state, the mole fraction of nitrogen molecules is lower than the equilibrium composition at that temperature and pressure. The system is initialized with translational  $T_t$ , rotational  $T_r$ , and vibrational temperature  $T_v$  all set to 2000 K. The initial total mass density corresponds to  $1.25 \text{ kg/m}^3$  with molecular mole fraction of 0.052 63 with 100 000 simulated atoms. These conditions promote rapid  $N_2$  recombination early on, as seen by the increase in the concentration of nitrogen molecules with time ( $x_{N_2}$ ) in Fig. 11. The recombination releases thermal energy into the gas, which quickly

increases the translational, rotational, and vibrational temperature of the system, shown by the solid red, blue, and black lines, respectively in Fig. 11. Early on, the vibrational temperature increases at a much higher rate than the other two temperatures. However, a small early overshoot of  $T_r$  relative to  $T_t$  can also be observed. Eventually, all three

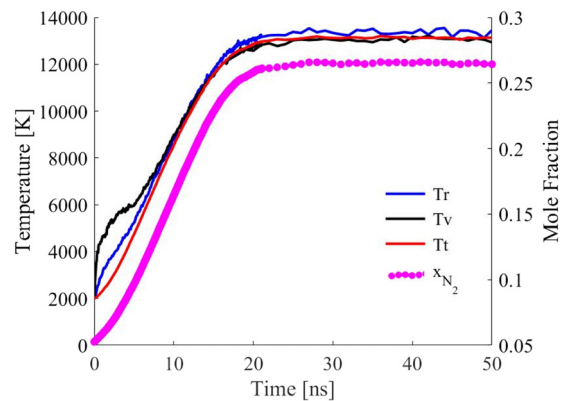


**FIG. 11.** Case 2: Adiabatic recombination-dominated relaxation. Initial state:  $T_t = T_r = T_v = 2000 \text{ K}$ ,  $\rho = 1.25 \text{ kg/m}^3$ ,  $x_{N_2} = 0.052 63$ . Translational, rotational, and vibrational temperature are depicted by solid red, blue, and black, respectively. Pink circles depict mole fraction of molecular nitrogen.

Downloaded from http://pubs.aip.org/aip/pof/article-pdf/doi/10.1063/5.0150492/17945365/067111\_1\_5.0150492.pdf

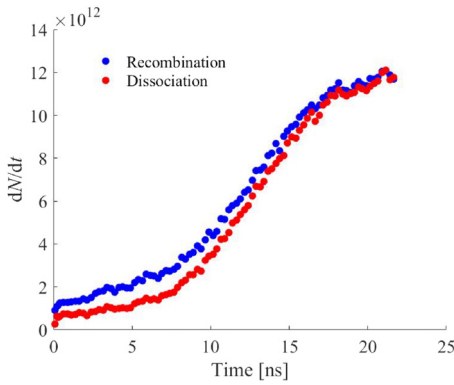


**FIG. 12.** Case 2: Adiabatic recombination-dominated relaxation. Time evolution of number of dissociations and recombinations per unit time.

temperatures equalize and continue to increase at the same rate. To some extent, relaxation of the rotational mode is slightly faster than vibrational, but overall rovibrational relaxation is rapid.

Figure 11 also shows the composition history obtained from MD (solid pink circles), which predicts a change of curvature of the mole fraction profile at the initial stage during evolution. It follows an “s-shape” curve where the initial production rate of nitrogen molecules is lower. A state-to-state study by Colonna *et al.*<sup>42</sup> also reported a similar qualitative s-shape trend of their atomic nitrogen mole fraction profile in the recombination-dominated regime. This s-shape feature is also evident in Fig. 12, which shows the rate of the forward and reverse reactive processes under these conditions. It shows that both recombination and dissociation follow a similar trend, with the recombination rate being a little higher than dissociation in the early stages. This difference narrows to zero as the system evolves and reaches equilibrium. The overall rate evolution can be divided into three stages. In the first stage between  $t = 0$  and  $t = 10$  ns, the system sees a slow rise in reactive processes. This is followed by a constant linear increase in

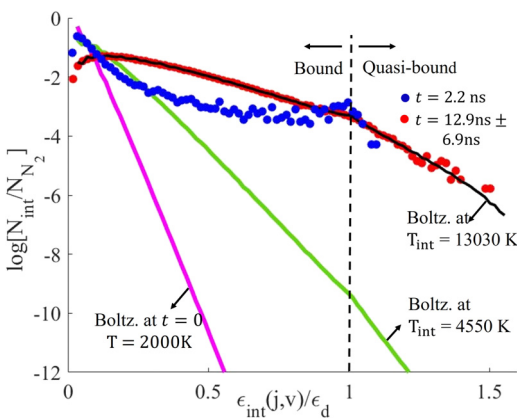


**FIG. 13.** Case 2: Adiabatic recombination-dominated relaxation. Time evolution of rovibrational energy population distributions (blue and red circles). Pink line depicts theoretical Boltzmann distribution at  $t = 0$ . Green and black lines: Boltzmann distribution at local internal temperature  $T_{int}$ .

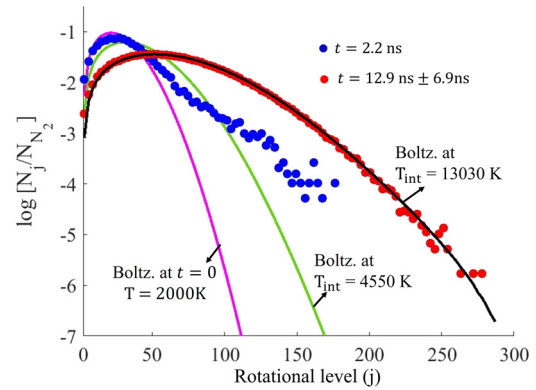


**FIG. 14.** Case 2: Adiabatic recombination-dominated relaxation. Time evolution of rotational population distribution functions (blue and red circles). Pink line depicts theoretical Boltzmann distribution at  $t = 0$ . Green and black lines: Boltzmann distribution at local internal temperature  $T_{int}$ .

recombination and dissociation in the second stage. In the final stage approximately starting at  $t = 20$  ns, both rates converge to the same value and the system reaches a steady state.

We present population distributions extracted at different time instants during the evolution in Figs. 13–15. To reduce statistical noise, we perform ensemble-averaging over three simulations where initial positions and velocities of atoms are extracted using random seeds (different microscopic states) at the same macroscopic conditions (density, temperature). This sums the total number of simulated atoms to 300 000.

For reference, we plot the equilibrium distribution (solid pink line) at  $t = 0$  ( $T = 2000$  K). The population distribution extracted from MD quickly becomes non-Boltzmann (blue solid points) at  $t = 2.2$  ns and shows a cusp near the dissociation limit of the  $N_2$  molecule. Figures 14 and 15 show the corresponding vibrational and rotational population distributions, where rovibrational energies are binned based on vibrational and rotational numbers, respectively. The rotational number-based distribution possesses significant non-Boltzmann

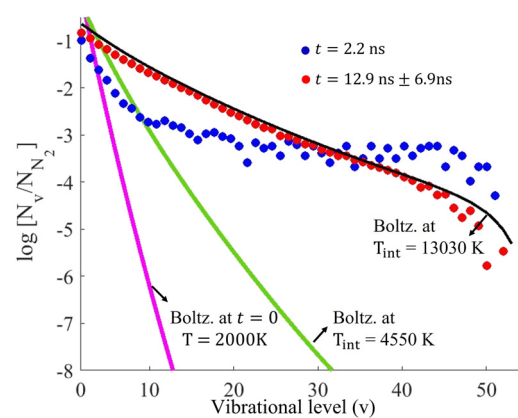


**FIG. 15.** Case 2: Adiabatic recombination-dominated relaxation. Time evolution of vibrational population distribution functions (blue and red circles). Pink line depicts theoretical Boltzmann distribution at  $t = 0$ . Green and black lines: Boltzmann distribution at local internal temperature  $T_{int}$ .

Downloaded from http://pubs.aip.org/aip/pof/article-pdf/doi/10.1063/5.0150492/17945365/067111\_1\_3.0150492.pdf



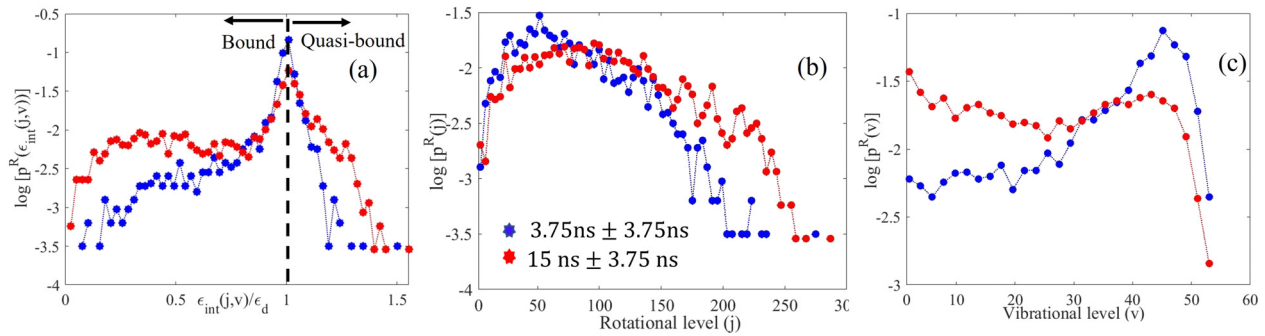


**FIG. 16.** Case 2: Adiabatic recombination-dominated relaxation. Time-averaged evolution of recombination probability density to a given (a) internal energy, (b) rotational, and (c) vibrational state, respectively. Blue and red circles depict density time-averaged over two distinct intervals (1 : [0, 11.25 ns]) and 2 : [11.25, 18.75 ns]), where  $(T_{t_2} > T_{t_1})$ .

character during early stages, where we see overpopulation of high and low rotational levels and a dip in between as compared to local equilibrium Boltzmann at  $T_{int} = 2000$  K. We also see a long plateau in the vibrational energy distribution, which happens due to the majority of preferential recombination into higher-lying vibrational levels. As time evolves, the distribution starts converging to the Boltzmann distribution (red circles).

Another characteristic of a recombining non-equilibrium gas is also observed in the evolution of the recombination probability density shown in Fig. 16. Figure 16(a) shows the probability that atoms will recombine to a particular internal energy state at two time instants  $t_1 = 3.75 \text{ ns} \pm \Delta t$  (blue circles) and  $t_2 = 15 \text{ ns} \pm \Delta t$  (red circles). These times correspond to different states where the translational temperature at  $t_2$  is higher than  $t_1$  ( $T_{t_2} > T_{t_1}$ ). It shows that the likelihood of a molecule recombining into a state close to the dissociation limit is high, and the translation temperature increases, the recombination PDF flattens, increasing the contribution of quasi-bound and bound states lying away from  $D^0$ . This suggests that the microscopic selectivity of recombination for certain energy levels is stronger at lower translational temperature. Figures 16(b) and 16(c) also show the corresponding PDFs with respect to rotational and vibrational quantum numbers. At  $t = t_1$ , the majority of recombined molecules have high vibrational and intermediate rotational numbers. As  $T_t$  increases, more molecules start appearing at low  $v$ . Simultaneously, the rotational recombination probability function shifts toward the right and flattens. Over time this microscopic bias of the recombining gas explains the

cusp in the instantaneous snapshot of internal energy population distribution and significant non-Boltzmann character of rotation, vibration-based population distributions analyzed in Figs. 13–15. A similar trend is also reported in previous work based on theoretical analysis using principle of microscopic reversibility.<sup>5</sup>

For completeness, Fig. 17 shows the dissociation probability density at the same times as that of the recombination PDFs. During the first time interval, the distribution in Fig. 17(a) exhibits a similar behavior, where the majority of pre-dissociation reactants are clustered near the  $\epsilon_{int}(j, v) = \epsilon_d$  curve, but the contribution of bound states is exceedingly small and the drop is sharp away from  $D^0$ . This is due to the combination of a low translational temperature and low mole fraction of molecular nitrogen. This behavior has some disparity in comparison to the case of the dissociation dominated regime investigated in Sec. III. As time evolves and the gas comes closer to an equilibrium state, the dissociating PDF (red solid circles in Fig. 17) begins to resemble the recombination PDF (red solid circles in Fig. 16) as expected.

The evolution of microscopic recombination and dissociation probability densities investigated in this and earlier sections showed that a major part of the energy during reactive processes is contributed by molecules populating levels close to the dissociation energy limit. This implies that the vibrational energy of dissociating and recombining molecules is higher than the average vibrational energy of molecules in the reactor, which in turn explains the higher instantaneous  $T_v$  relative to the other energy modes early on in Fig. (11).

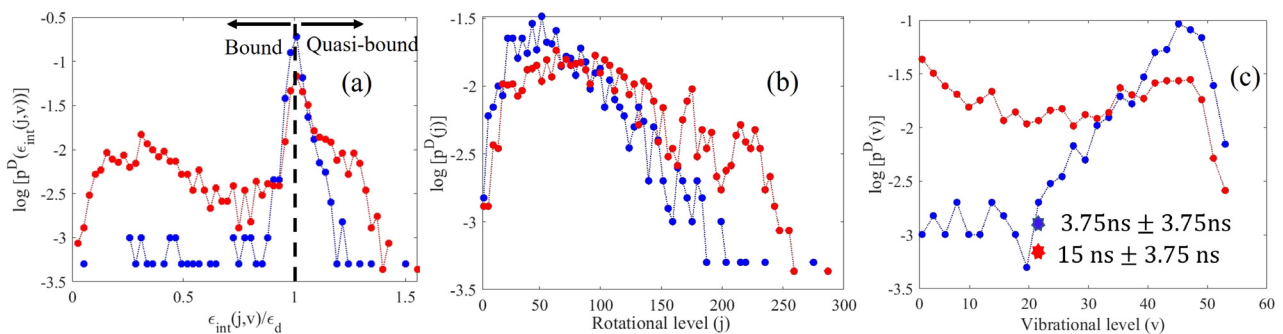


**FIG. 17.** Case 2: Adiabatic recombination-dominated relaxation. Time-averaged evolution of dissociation probability density from a given (a) internal energy, (b) rotational, and (c) vibrational state, respectively. Blue and red circles depict density time-averaged over two distinct intervals (1 : [0, 11.25 ns]) and 2 : [11.25, 18.75 ns]), where  $(T_{t_2} > T_{t_1})$ .

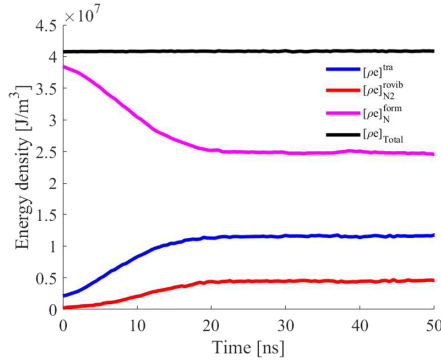


**FIG. 18.** Case 2: Adiabatic recombination-dominated relaxation. Time history of different components of energy for a system under recombination-dominated regime.

In conclusion, the microscopic physics of chemistry guides the evolution of macroscopic profiles, which motivate first-principle based modeling development for higher-scale theories like DSMC and CFD. A few such efforts have been made in Refs. 5, 6, and 43–46.

Figure 18 shows the evolution of different components of energy density as time progresses. The total energy of the system is a summation of these different components, which include the kinetic energy per unit volume of particles due to thermal motion relative to each other  $[\rho e]^{tra}$ , rovibrational energy density of molecular nitrogen  $[\rho e]_{N_2}^{rovib}$ , and formation energy per unit volume of atomic nitrogen  $[\rho e]_N^{form}$ ,

$$[\rho e]_{Total} = [\rho e]^{tra} + [\rho e]_{N_2}^{rovib} + [\rho e]_N^{form} = \frac{3}{2} \left( \frac{\rho_{N_2}}{M_{N_2}} + \frac{\rho_N}{M_N} \right) RTt + [\rho e]_{N_2}^{rovib} + \rho_N h_N^0, \quad (2)$$

$h_{N_2}^0 = 0$  and  $h_N^0 = D^0/2$ ,  $R$  is the universal gas constant, and  $M_s$  is mass per unit mole of species  $s$ . Since the bulk velocity  $v$  is set to zero initially and remains conserved, the contribution of the bulk kinetic energy, i.e.,  $\frac{1}{2} \rho v^2$ , has been ignored. As the gas evolves over time, the

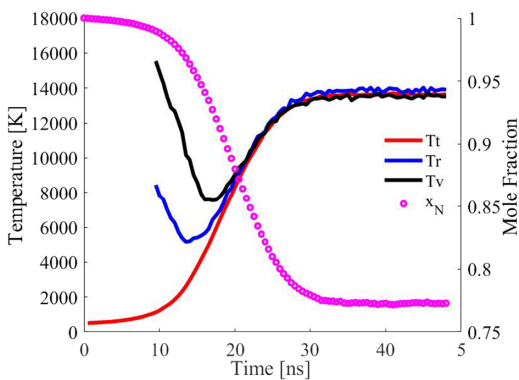


**FIG. 19.** Case 2: Adiabatic recombination-dominated relaxation. Time history of various temperatures and atomic mole fraction of a system, initially composed of atomic nitrogen  $x_N = 1$ , at the initial temperature of 500 K.

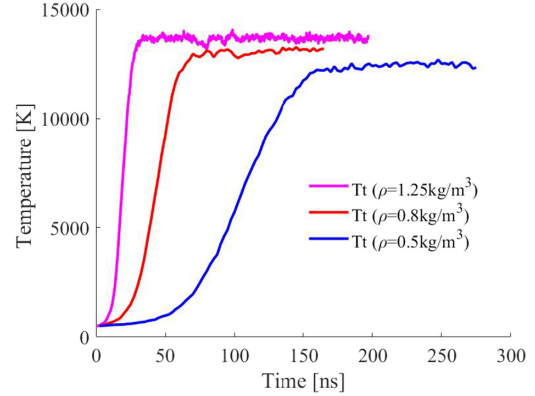


**FIG. 20.** Case 2: Adiabatic recombination-dominated relaxation. Comparison of the evolution of translational temperature between adiabatic reactors of different densities. Initial state:  $x_N = 1$ ,  $T = 500$  K.

translational temperature and mole fraction of molecular nitrogen increases. This results in an increase in thermal and rovibrational energy and a decrease in the formation energy of atomic nitrogen. The total energy of the system remains conserved, as expected. We emphasize that  $A$  is identically zero for the adiabatic system investigated in this section, i.e., there is no flow.

Next, we simulate an adiabatic reservoir composed of all nitrogen atoms ( $x_N = 1$ ) at an initial temperature of  $T = 500$  K. The total mass density is set to  $1.25 \text{ kg/m}^3$ . As time evolves, nitrogen atoms recombine, decreasing the atomic mole fraction (pink circles in Fig. 19), which follows an s-shape profile similar to the one seen in the earlier example in Fig. 11. Corresponding to this, the translational temperature rises with time. Internal temperatures of the system are only computed once a sufficient number of molecules appear in the system. As atoms recombine, the rotational and vibrational temperatures start out from high values due to the microscopic selectivity of chemistry, and begin by decreasing before their eventual equilibration with the translational mode. Another important result is shown in Figs. 20 and 21, which show the time evolution of translational temperature and atomic mole fraction of systems initialized at different densities under recombination dominated regimes. It is observed that with an increase in density, the temperature of the final steady state attained increases and the corresponding final mole fraction of atomic nitrogen decreases. The system with lowest density of  $0.5 \text{ kg/m}^3$  takes the longest time to approach the thermo-chemical equilibrium state. This is to be expected, since the relaxation rates scale with collision rate, which itself scales with the square of density.

### V. OMD REACTOR

In this section, we study sudden compression and sudden expansion processes. To do so, we study the non-equilibrium evolution of nitrogen gas in an OMD reactor where  $A$  is chosen to be

$$\mathbf{A} = \kappa \mathbf{e}_1 \otimes \mathbf{e}_1 + \kappa \mathbf{e}_2 \otimes \mathbf{e}_2 + \kappa \mathbf{e}_3 \otimes \mathbf{e}_3. \quad (3)$$

Recall that the macroscopic velocity field  $\mathbf{v}(\mathbf{x}, t) = \mathbf{A}(\mathbf{I} + t\mathbf{A})^{-1}\mathbf{x}$  of OMD is a special, but also an exact solution of the equations of continuum fluid mechanics. The set of ODEs that correspond to reduced fluid dynamics modeling of an OMD reactor is given in the

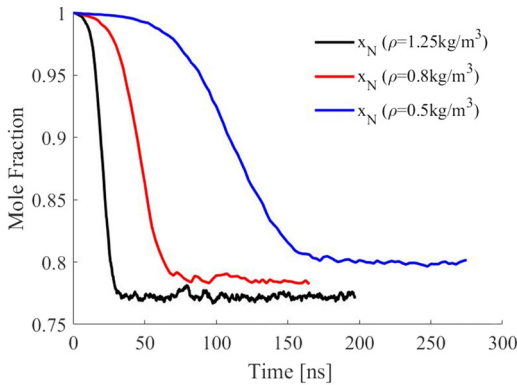


**FIG. 21.** Case 2: Adiabatic recombination-dominated relaxation. Comparison of the evolution of atomic mole fraction between adiabatic reactors of different densities. Initial state:  $x_N = 1$ ,  $T = 500$  K.

Appendix [Eq. (A4)]. The chosen value of the A tensor for the system investigated in this work simplifies to

$$\begin{aligned} \frac{d\rho_{N_2}}{dt} + \rho_{N_2} \frac{3\kappa}{\kappa t + 1} &= w_{N_2}, & \frac{d\rho_N}{dt} + \rho_N \frac{\kappa}{\kappa t + 1} &= w_N \\ \frac{de}{dt} + \left( (e + \tilde{p}) \frac{3\kappa}{\kappa t + 1} \right) &= 0, & \frac{de_v}{dt} + e_v \frac{3\kappa}{\kappa t + 1} &= w_v, \end{aligned} \quad (4)$$

where the velocity field has been substituted with  $\mathbf{v} = \frac{3}{\kappa t + 1} \mathbf{A} \mathbf{x}$  in Eq. (A4). The chosen flow is the simplest OMD case of pure dilatation where the traceless symmetric part of the velocity gradient tensor  $\mathbf{E} = \frac{1}{2}(\nabla \mathbf{v} + \nabla \mathbf{v}^T) - \frac{1}{3}(\nabla \cdot \mathbf{v})\mathbf{I}$  and, hence, Newtonian viscous stress tensor  $\boldsymbol{\tau}$  are identically zero for fluids whose bulk viscosity vanishes. It is known from previous studies that under strong gradients, the Chapman–Enskog closure leading to Navier–Stokes–Fourier equations breaks down.<sup>1</sup> Choosing this special family of pure uniform dilatation in the framework of OMD allows us to remove the extra complexity of the presence of non-Newtonian momentum and possible non-Fourier energy transport contributed from E and temperature gradients in the system.

Note that it is assumed that Stokes’ hypothesis holds true when deriving Eq. (4) for nitrogen gas. This assumption being valid for a dilute mono-atomic gas as predicted by kinetic theory and experiments<sup>47</sup> might not hold true for diatomic systems with large dilatation, which results in an added effect of non-zero bulk viscosity in the total energy conservation equation.<sup>48</sup> Under those conditions,  $p$  is given by  $p = \frac{1}{3} \text{tr}(\boldsymbol{\sigma})\mathbf{I}$ , which is not necessarily equal to thermodynamic pressure  $\tilde{p}$  defined by perfect gas law with respect to translational-rotational temperature. Additionally under strong velocity gradients (large  $\kappa$ ) considered in this work, the system experiences a large departure from equilibrium due to which  $p$  may not be simply equal to  $(\tilde{p} + (\lambda + \frac{2}{3}\mu) \nabla \cdot \mathbf{v})$ . In fact, the definition of bulk viscosity as a physical property of the gas itself is questionable under strong non-equilibrium conditions. It is shown in Ref. 49 that bulk viscosity is an approximation designed to simulate the effect of thermal relaxation when the state of gas is described by governing equations in terms of a single temperature. This is based on the assumption of fast relaxation of rotational mode in comparison with the timescale of the flow. In a highly non-equilibrium regime, this assumption breaks down and a

separate rotational energy conservation equation is required to more accurately characterize the state of the gas.

### A. Compression and relaxation of nitrogen gas in an OMD reactor

In this subsection, we study the non-equilibrium evolution of relatively cold gas under sudden uniform compression followed by relaxation. This is achieved by first setting  $\kappa$  to  $-5 \times 10^8 \text{ s}^{-1}$  during compression and then switching to 0 in Eq. (3) for relaxation. The initial temperature and mass fraction corresponds to an equilibrium system of cold nitrogen gas at 300 K with initial total mass density of  $\rho(0) = 1.25 \times 10^{-3} \text{ kg/m}^3$  and  $y_{N_2} = 1$ . Macroscopic profiles and population distributions are extracted by doing ensemble averaging over five trajectories of 10 000 simulated atoms. The initial population follows a Maxwell–Boltzmann distribution at this temperature. The system mimics the behavior of gas traversing a shock front and immediately downstream in the temporal frame where the transient behavior of the system can be mapped to several locations across the shock wave.

In Fig. 22, we plot the OMD evolution of translational, internal temperatures, and the mass fraction of nitrogen molecules ( $y_{N_2}$ ). The solid lines represent the evolution in the compression phase, whereas the dashed lines show the relaxation regime. Note that a little higher  $T_v$  than 300 K at  $t = 0$  is an artifact of the classical approach for vibrational energy determination, which is significant at lower temperatures. During the compression phase, the translational temperature increases rapidly, whereas the excitation of the internal energy mode is slower. This results in strong thermal non-equilibrium between the translational, rotational, and vibrational energy modes of the gas as also observed in the previous shock-tube experiment study.<sup>50</sup> It is observed that the dissociation of the gas does not initiate until the vibrational mode is sufficiently excited, which mainly happens in the relaxation phase.

During relaxation, the internal energy modes become excited and the gas immediately starts dissociating, which removes translational and internal energy from the system. We observe that the equilibration of rotational and translational energies is more rapid than equilibration of the vibrational energy. The rotational temperature increases

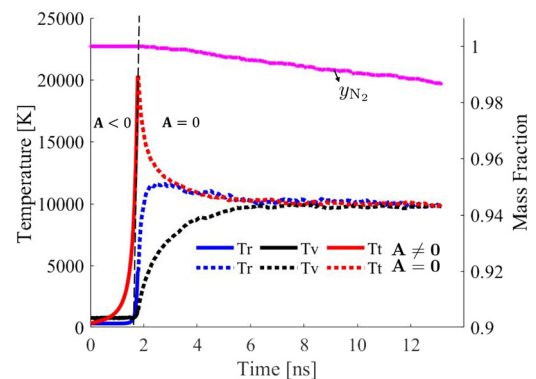


**FIG. 22.** Case 3: Compression and relaxation in the OMD reactor. Time history of mass fraction of molecular nitrogen, system translation temperature, and rotational and vibrational temperature during compression  $A < 0$  and relaxation regime  $A = 0$ .

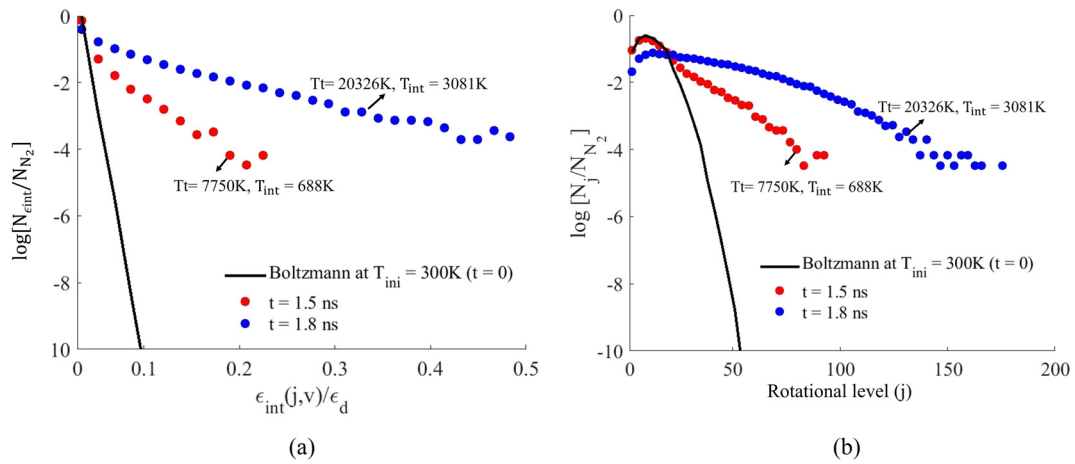


**FIG. 23.** Case 3: Compression and relaxation in the OMD reactor. Evolution of (a) rovibrational energy and (b) rotational number binned populations (blue and red circles) during compression. Black line depicts theoretical Boltzmann distribution at  $t = 0$ .

and equilibrates with translational temperature at about 11 150 K, followed by equilibration with the vibrational temperature at about  $T_t \approx T_r \approx T_v \approx 9765$  K. Only about 3% of dissociation happens in this rovibrational excitation period, whereas the majority of reactive collisions occur in a regime where all the energy modes are in near-thermal equilibrium with each other and is cooling gradually. Thus, the internal energy relaxation and reactive zones are roughly separated. A careful choice of the A tensor and time duration of the compression regime can qualitatively provide different non-equilibrium behavior of a gas under different strengths (enthalpy) of the shocks. During the course of simulation, total density  $\rho = \rho_{N_2} + \rho_N$  of the system increases in the compression regime abruptly over a short period of time. This is given by Eq. (A5), which simplifies to  $\rho_t = \frac{\rho_0}{(\kappa t + 1)^3}$  for a uniform dilatation.

Further insight may be gained by examining the evolution of the population distribution based on internal energy and rotational and vibrational quantum numbers during the compression phase as shown in Figs. 23 and 24(a). In the early stages of the compression, due to a faster rise of translational temperature compared to rotation and vibration, we see non-Boltzmann-like behavior with higher internal energy; also, higher-lying rotational and vibrational states become rapidly over-populated as the gas evolves. The higher-lying levels become more populated the further the gas becomes excited in the compression regime. These features are in line with what has been observed in previous DMS and state-resolved master equation studies of shock waves.<sup>51,52</sup> The disruption of rotational number-binned population distribution in Fig. 23(b) relative to the equilibrium distribution at  $t = 0$  starts from levels with lower quantum numbers as the gas evolves

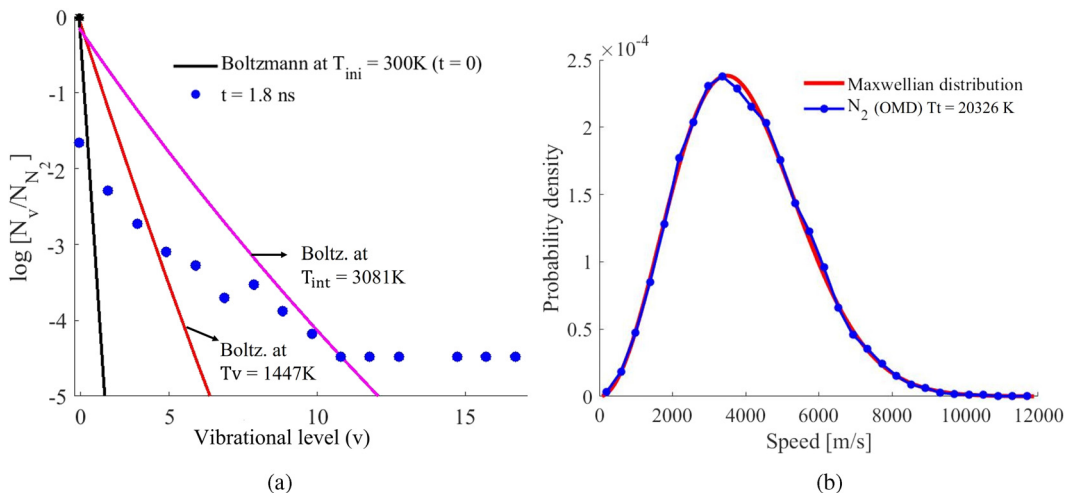


**FIG. 24.** Case 3: Compression and relaxation in the OMD reactor. (a) Vibrational population distribution function (blue circles) for molecules at the end of compression. Black line depicts theoretical Boltzmann distribution at  $t = 0$ . Red and pink solid lines: Boltzmann distribution at local vibrational  $T_v$  and internal temperature  $T_{int}$ , respectively. (b) Speed distribution of  $N_2$  molecules at the end of compression regime. The solid red lines represent Maxwellian distributions at instantaneous  $T_t$ .

under compression, thus eventually reaching a distribution that is far-from-Boltzmann. Figure 24(a) shows the vibrational number based population distribution at the end of the compression phase. (This is before  $T_v$  has reached its maximum.) It is evident from the plot that in the current situation, a local Boltzmann-like vibrational-binned distribution at a characteristic vibrational temperature  $T_v$  or an internal temperature  $T_{int}$  would be insufficient to accurately characterize this non-equilibrium physics. The OMD-computed distribution (in blue solid circles) shows significant departure from Boltzmann statistics. Thus, in this regime, if a Boltzmann distribution at  $T_v$  is assumed, the dissociation rate would be under-predicted, since the high-energy states are exponentially more likely to dissociate. The time history of the population distributions in the relaxation regime is omitted here due to its similarity with the behavior of a gas under adiabatic conditions in the dissociation-dominated regime investigated in Sec. IV. Finally, Fig. 24(b) shows the speed distribution of  $N_2$  molecules at an instant where the gas is in a highly compressed state. The fact that the OMD-derived speed distribution almost exactly matches the local Maxwellian at  $T_t$  shows the rapid relaxation of the translational mode of the gas. Note, however, that the distribution can strongly deviate when one makes the different choice of flow as in our earlier work,<sup>2</sup> where, by choosing the tensor  $A$  differently, one can see translational non-equilibrium when the velocity distribution departs significantly from the local equilibrium Maxwellian.

### B. Expansion and relaxation of nitrogen gas in an OMD reactor

The simulation of expansion and subsequent adiabatic relaxation with OMD are achieved by choosing the same form of  $A$  as done in the previous case, except we choose  $\kappa$  to be positive ( $\kappa = 5 \times 10^9 \text{ s}^{-1}$ ), which results in the enlargement of the fundamental domain of simulated atoms with time. This setting qualitatively mimics the behavior of gas in a nozzle expansion, but represented in the time domain. We start the analysis with the partially dissociated gas at thermal equilibrium at 10 000 K with  $\rho^0 = 10 \text{ kg/m}^3$  and 50% diatomic nitrogen (by mass fraction) and 100 000 simulated atoms. A higher initial density is chosen to capture the noticeable impact of recombination reactions on the behavior of the expanding gas already within the timescale of MD.

The temperature and mass fraction evolution during the expansion and relaxation regimes are plotted in Fig. 25. Contrary to the previous case, the sudden expansion leads to rapid cooling, which decreases the translational temperature followed by the rotational and vibrational temperatures. During expansion, a large drop in the gas density and temperature decreases the collision rate, which results in much slower relaxation of the rotational and vibrational temperatures. This leads to situation where  $T_r$  and  $T_v$  lag the change in  $T_t$ , i.e.,  $T_t < T_r < T_v$  at the end of the expansion phase. During this time, the atomic nitrogen recombines and the mass fraction of molecular nitrogen increases relatively quickly (purple stars in Fig. 25), followed by its freezing later on (purple squares). This is reminiscent of the behavior observed downstream of the throat of a nozzle. In the relaxation regime, the translational mode slowly excites (dashed red line) and internal energy modes (dashed blue and black lines) relax. We see that rotational temperature is equilibrated with the translational temperature, first at about  $\approx 4703 \text{ K}$ , followed by the vibrational temperature at about  $\approx 5010 \text{ K}$ . The dynamics of gas in the relaxation regime is slower due to a lower mass density which resulted from the expansion [ $\rho_t = \frac{\rho_0}{(\kappa t + 1)^3}$ ].

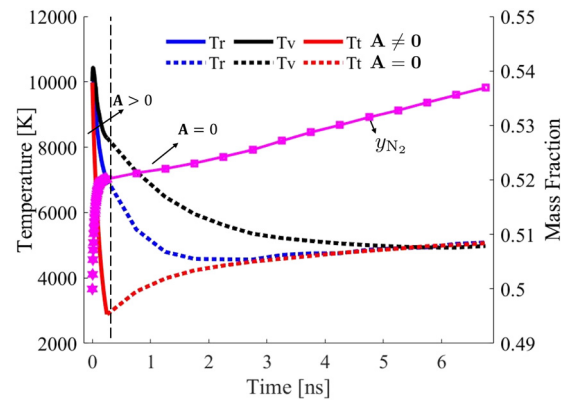


FIG. 25. Case 4: Expansion and relaxation in the OMD reactor. Expansion and relaxation in OMD reaction: Time history of mass fraction of molecular nitrogen, system translation temperature, rotational and vibrational temperature during expansion  $A > 0$  and relaxation regime  $A = 0$ .

This is evident from the slow recombination and rate change of temperature as compared to dynamics in the first 0.2 nanoseconds of expansion.

Next, we show the evolution of population distributions evolution in Figs. 26(a), 26(b), and 27(a). At  $t = 0$ , we have a Boltzmann distribution at the given equilibrium temperature of 10 000 K (solid black line). As time evolves, the internal energy distributions show a strong cusp near the dissociation limit due to the tendency of molecules to recombine into these high energy levels. Low-lying internal energy states in Fig. 26(a) are in thermal equilibrium at an internal temperature where they follow a Boltzmann distribution (solid black and green lines) plotted at local internal temperature ( $T_{int}$ ). High-lying states are overpopulated and the distribution deviates from a Boltzmann-like shape. This disruption starts to affect increasingly lower levels as the gas evolves and expands. Corresponding to this, the populations of low and high-lying rotational states are higher as compared to the Boltzmann distribution at  $T_{int}$  as shown in Fig. 26(b).

The vibrational distributions in Fig. 27(a) start relaxing from the tails and show a characteristic “L-shape” driven by the dominance of recombinations, vibration-to-vibration energy exchange (V-V) and vibration-to-translation (V-T) relaxation processes.<sup>33</sup> The plateau in the high energy tails of the distributions becomes longer as time evolves while the populations of low-lying levels remain almost constant. The local Boltzmann distributions at  $T_{int}$  shown by the solid black and green lines (local Boltzmann at the extreme extent of expansion) lie significantly below the OMD populations for high-lying vibrational levels and are a little higher for low-lying levels. The departure from Boltzmann statistics for low-lying levels is less extreme in comparison with a gas under compression, investigated in the previous case. Overall, one can see the qualitative similarity of the OMD computed vibrational distribution reported here with state-to-state modeling and experimental studies undertaken to study nozzle expansion and nonequilibrium vibrational kinetics in the literature.<sup>33,52,53</sup> These strong non-equilibrium distributions can directly influence the corresponding energy transfer and reaction rates as investigated in Refs. 33, 54, and 55.

As the relaxation process continues and the gas slowly recombinates, we see that the non-equilibrium behavior of the gas reaches

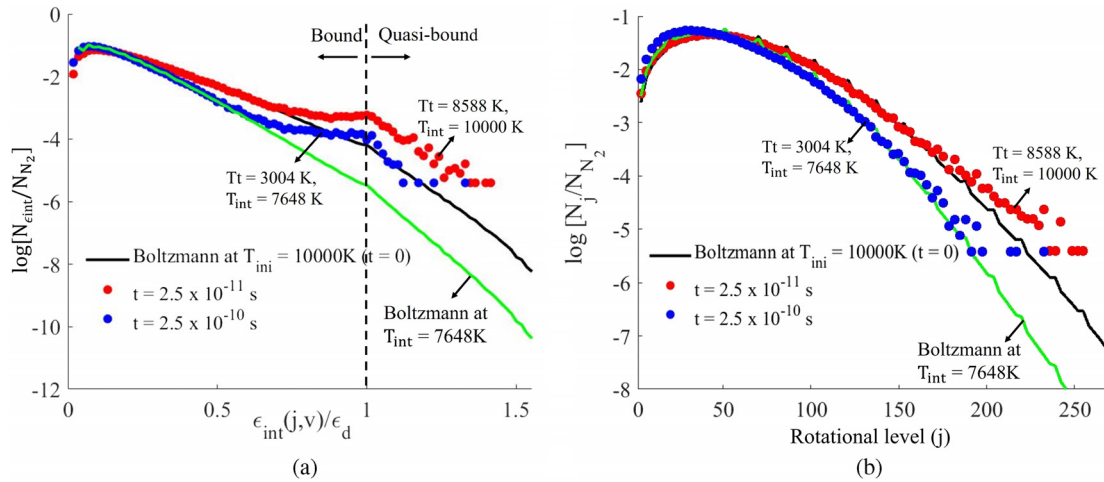


FIG. 26. Case 4: Expansion and relaxation in the OMD reactor. Evolution of (a) rovibrational energy and (b) rotational number binned populations (blue and red circles) during expansion. Black (equilibrium distribution at  $t = 0$ ) and green lines: theoretical Boltzmann distribution at local internal temperature  $T_{int}$ .

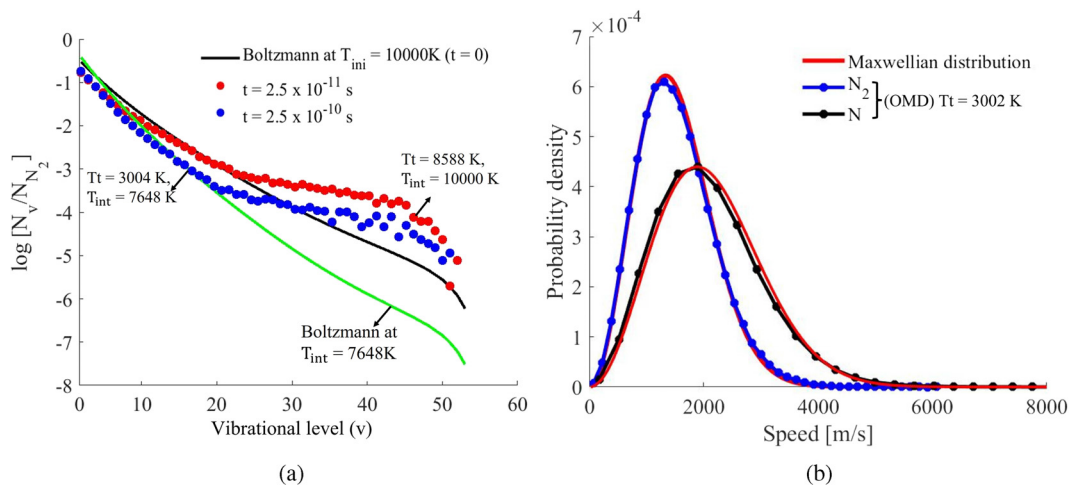


FIG. 27. Case 4: Expansion and relaxation in OMD reactor. (a) Evolution of vibrational population distribution functions (blue and red circles) for molecules during expansion. Black (equilibrium distribution at  $t = 0$ ) and green lines: theoretical Boltzmann distribution at local internal temperature  $T_{int}$ . (b) Speed distribution of  $N_2$  molecules (dashed-circle blue line) and N (dashed-circle black line) atoms at the end of expansion. The solid red lines represent Maxwellian distributions at instantaneous  $T_t$ .

a quasi-steady state (QSS), where the population distribution becomes time invariant due to balance between inelastic and recombinative collisional process. In this region, the high internal energy, rotational and vibrational tails are overpopulated relative to the corresponding Boltzmann distribution at  $T_t \approx T_r \approx T_v \approx 5280$  K, as shown in Fig. 28. Figure 27(b) shows the speed distribution of  $N_2$  and N at the end of the expansion regime. At this instant, the gas is still in a state of thermal and chemical non-equilibrium where the translational and internal temperatures of the gas are different. However, at the end of the expansion phase, the instantaneous distributions of  $N_2$  and N already follow the Maxwell-Boltzmann distribution closely within statistical uncertainty. This shows that the translational mode rapidly relaxes to the local equilibrium speed distribution defined at the corresponding instantaneous translation temperature of the system.

## VI. SUMMARY AND CONCLUSIONS

To our knowledge, this is the first pure MD study that simulates the concurrent processes—dissociation, recombination, and exchange as they happen in a nitrogen gas evolving under non-equilibrium conditions, based on an *ab initio* (first-principles calculations) dataset derived reactive force field. Collision dynamics naturally include three-body collisions due to  $N + N + N$  and  $N_2 + N + N$ , as well as rare many-body collisions. The vibrational population distributions observed in this work reveal significant non-Boltzmann features during relaxation of the gas in adiabatic and non-adiabatic reactor under recombination and dissociation-dominated regimes.

An analysis of the probability densities for recombination and dissociation suggests microscopic selectivity of these processes, where favoring of certain rovibrational states is observed. On the other hand,

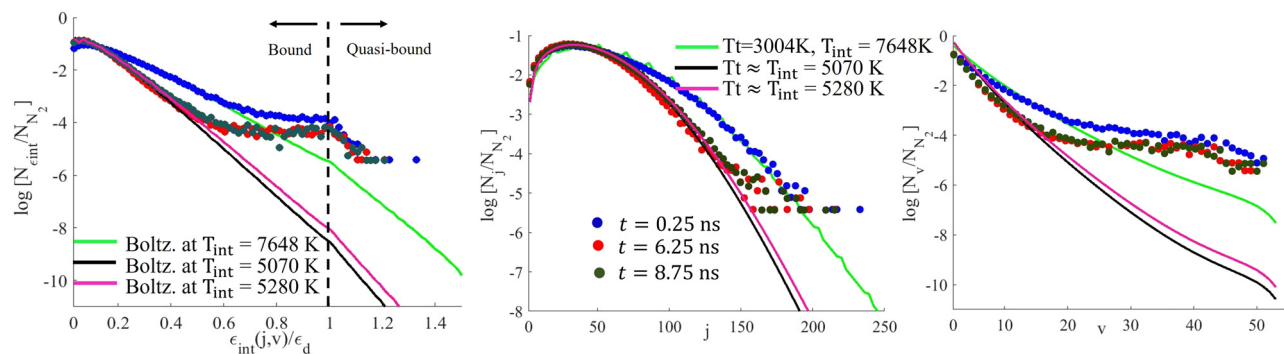


**FIG. 28.** Case 4: Expansion and relaxation in OMD reactor. Evolution of internal energy, rotational and vibrational population distribution functions (solid circles) for molecules during relaxation. Green (equilibrium distribution at the extreme extent of expansion), black and magenta lines: theoretical Boltzmann distribution at local internal temperature  $T_{int}$  during relaxation.

the exchange process shows no bias and, hence, its post-collision rovibrational probability density resembles the instantaneous population distribution of molecular nitrogen in the mixture.

The net dissociation probability density in the non-equilibrium gas is an aggregate effect of the instantaneous population distribution of molecules and the selectivity of dissociation. It is observed that nitrogen gas tends to dissociate from states whose energy is close to the dissociation energy of the  $N_2$  molecule ( $D^0$ ) and from those which have high vibrational number. As the temperature increases, more and more molecules in low-lying internal energy states collide with enough translational energy to overcome the dissociation barrier, causing the dissociation PDF to become more uniform. Similarly, atoms have a tendency to recombine into molecules populating close to the dissociation limit, with high vibrational and intermediate rotational quantum numbers. As the temperature increases, the probability density function flattens and the probability of recombining into states far from  $D^0$  increases. On the vibrational and rotational recombination PDFs, this corresponds to an increase in the contribution of low vibrational and high rotational numbers, thus making the whole vibrational manifold attain a more uniform probability.

We have introduced the method of objective molecular dynamics for the study of reacting gas mixtures out of thermo-chemical equilibrium resembling the conditions encountered in high-temperature flows. OMD simplifies the MD simulation of space-homogeneous reservoirs to a great extent by naturally enforcing time-dependent periodicity in all spatial direction. This makes the use of the deterministic non-equilibrium molecular dynamics approach more affordable. Note that OMD makes no assumptions on the dynamics of atoms, and each and every atom (simulated and non-simulated) satisfies the MD equations exactly for their forces. This also holds true at the discrete level when using the velocity-Verlet algorithm as shown in Ref. 25. Several special choices of the OMD family of motions make it possible to more closely mimic the nonequilibrium chemistry in nozzle expansion or shock layers than would be possible by assuming adiabatic or isothermal conditions. In addition, the fact that OMD simulates motions, which are exact solutions of the momentum conservation equation of fluid dynamics, encourages its use to propose and test new transport, energy relaxation, and chemical kinetics models, in the framework of reduced CFD for which an exact atomistic analog exists. The illustration of the method in this study has only focused on one

special choice of A tensor (uniform dilatation). The full family of velocity fields given by  $\mathbf{v} = \mathbf{A}(\mathbf{I} + t\mathbf{A})^{-1}\mathbf{x}$  is quite broad, and its scope includes many other examples of steady and unsteady compressible and incompressible flows, including cases with time-dependent vorticity and cases with strong singularities.

From the analysis of underlying population distribution functions in the compression and expansion regime, we see significant non-Boltzmann, non-equilibrium features produced by the combination of selectivity of the chemistry and separation in the timescale of relaxation of different internal energy modes. It is shown that OMD analysis can produce all the relevant features and can provide the necessary details needed for higher-scale modeling. The method qualitatively reproduces the formation of an L-shape vibrational distribution with an overpopulation of high-lying vibrational states created by the recombination and energy exchange processes under expansion.

## ACKNOWLEDGMENTS

G. Pahlani and R. D. James acknowledge funding from the Multidisciplinary Research Program of the University Research Initiative (MURI) under Grant No. FA9550-18-1-0095 and a Vannevar Bush Faculty Fellowship (Grant No. N00014-19-1-2623). T. E. Schwartzentruber and E. Torres acknowledge funding from NASA under Grant No. 80NSSC20K1061.

## AUTHOR DECLARATIONS

### Conflict of Interest

The authors have no conflicts to disclose.

### Author Contributions

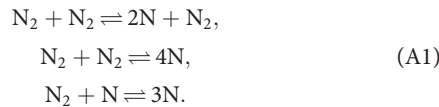
**Gunjan Pahlani:** Conceptualization (equal); Data curation (equal); Formal analysis (equal); Investigation (equal); Methodology (equal); Software (equal); Validation (equal); Visualization (equal); Writing – original draft (equal). **Erik Torres:** Supervision (equal); Writing – review & editing (equal). **Thomas E. Schwartzentruber:** Supervision (equal); Writing – review & editing (equal). **Richard D. James:** Conceptualization (equal); Formal analysis (equal); Funding acquisition (equal); Methodology (equal); Project administration (equal); Resources (equal); Supervision (equal); Writing – review & editing (equal).

DATA AVAILABILITY

The data that support the findings of this study are available from the corresponding author upon reasonable request.

APPENDIX: REDUCED FLUID DYNAMICS FOR OMD

Compressible flows of vibrationally excited and chemically reacting gases can be described by a two-temperature model (2T), where separate conservation equations for total energy and vibrational energy of the mixture are defined. This is to take into account possible thermal non-equilibrium between the translational and vibrational modes of the gas. This gives rise to two separate definitions of temperature: T for translational-rotational and Tv for vibrational temperature.<sup>56</sup> Additionally, mass conservation equations for every species with source terms containing reaction rates that govern the creation and removal of species are defined. In this study, we aim to investigate relaxation and reactive processes in Nitrogen gas only. The corresponding reaction set includes



The study takes into account both forward (dissociation) and backward (recombination) reactions. The corresponding conservation equations of fluid dynamics for two species N<sub>2</sub> and N take the form<sup>57</sup>

$$\begin{aligned} \frac{\partial \rho_{N_2}}{\partial t} + \nabla \cdot (\rho_{N_2} \mathbf{v}) &= -\nabla \cdot (\rho_{N_2} \mathbf{u}_{N_2}) + w_{N_2}, \\ \frac{\partial \rho_N}{\partial t} + \nabla \cdot (\rho_N \mathbf{v}) &= -\nabla \cdot (\rho_N \mathbf{u}_N) + w_N, \\ \frac{\partial \rho \mathbf{v}}{\partial t} + \nabla \cdot (\rho \mathbf{v} \otimes \mathbf{v} + p \mathbf{I}) &= \nabla \cdot \boldsymbol{\tau}, \\ \frac{\partial E}{\partial t} + \nabla \cdot ((E + p) \mathbf{v}) &= \nabla \cdot (\boldsymbol{\tau} \mathbf{v}) - \nabla \cdot (\mathbf{q}_t + \mathbf{q}_r + \mathbf{q}_v) \\ &\quad - \nabla \cdot (\rho_{N_2} h_{N_2} \mathbf{u}_{N_2} + \rho_N h_N \mathbf{u}_N), \\ \frac{\partial E_v}{\partial t} + \nabla \cdot (E_v \mathbf{u}) &= -\nabla \cdot \mathbf{q}_v - \nabla \cdot (\rho_{N_2} e_{N_2} \mathbf{u}_{N_2} + \rho_N e_N \mathbf{u}_N) + w_v, \end{aligned} \tag{A2}$$

where  $E = (\rho_{N_2} C_{vN_2} T + \rho_N C_{vN} T + E_{vN_2} \rho_{N_2} + h_{N_2}^o \rho_{N_2} + h_N^o \rho_N)$  and  $e_v = e_{vN_2} \rho_{N_2}$  are total energy and vibrational energy per unit volume, respectively,  $\rho = (\rho_{N_2} + \rho_N)$  is the total density,  $p$  is the trace of pressure tensor  $\boldsymbol{\sigma}$  [ $p = \frac{\text{tr}(\boldsymbol{\sigma})}{3}$ ],  $\boldsymbol{\tau}$  is the viscous stress tensor [ $\boldsymbol{\tau} = -(\boldsymbol{\sigma} - p \mathbf{I})$ ],  $\mathbf{q}_t, \mathbf{q}_r, \mathbf{q}_v$  are translational, rotational, and vibrational heat flux vectors,  $h_s^o$  is the formation enthalpy per unit mass of species  $s$ ,  $u_s$  is the species diffusion velocity,  $w_s$  is the rate of production of species  $s$  due to chemical reactions, and  $w_v$  is the vibrational energy source term.

These conservation equations are greatly simplified for OMD flows,  $\mathbf{v} = \mathbf{A}(\mathbf{I} + t\mathbf{A})^{-1} \mathbf{x}$ , where due to absence of any spatial dependencies, the PDEs of continuum mechanics reduce to a system of ODEs, heat flux vanishes, and the momentum conservation equation is identically satisfied for all accepted constitutive relations—Newtonian or non-Newtonian,<sup>19</sup> i.e.,

$$\begin{aligned} \frac{\partial \rho \mathbf{v}}{\partial t} + \nabla \cdot (\rho \mathbf{v} \otimes \mathbf{v}) &= \rho \left( \frac{d\mathbf{v}}{dt} + \nabla \mathbf{v} \mathbf{v} \right) \\ &= \rho (-\mathbf{A}(\mathbf{I} + t\mathbf{A})^{-1} \mathbf{A}(\mathbf{I} + t\mathbf{A})^{-1} \mathbf{y} \\ &\quad + \mathbf{A}(\mathbf{I} + t\mathbf{A})^{-1} \mathbf{A}(\mathbf{I} + t\mathbf{A})^{-1} \mathbf{y}) \\ &= \nabla \cdot \boldsymbol{\sigma} = 0. \end{aligned} \tag{A3}$$

Substitution of the macroscopic velocity field  $\mathbf{v}(\mathbf{x}, t) = \mathbf{A}(\mathbf{I} + t\mathbf{A})^{-1} \mathbf{x}$  of an OMD reactor into the PDEs of Eq. (A2) yields the following reduced system of ODEs for nitrogen gas:

$$\begin{aligned} \frac{d\rho_{N_2}}{dt} + \rho_{N_2} \text{tr}(\mathbf{A}(\mathbf{I} + t\mathbf{A})^{-1}) &= w_{N_2}, \\ \frac{d\rho_N}{dt} + \rho_N \text{tr}(\mathbf{A}(\mathbf{I} + t\mathbf{A})^{-1}) &= w_N, \quad w_{N_2} = -2w_N, \\ \frac{dE}{dt} + (E + p) \text{tr}(\mathbf{A}(\mathbf{I} + t\mathbf{A})^{-1}) &= (\mathbf{A}(\mathbf{I} + t\mathbf{A})^{-1}) \cdot \boldsymbol{\tau}, \\ \frac{dE_v}{dt} + E_v \text{tr}(\mathbf{A}(\mathbf{I} + t\mathbf{A})^{-1}) &= w_v. \end{aligned} \tag{A4}$$

The evolution of total density  $\rho_t$  of the mixture, which comes by summing species mass conservation equations in Eq. (A4), can be solved explicitly as a function of time. The solution is given by

$$\rho_t = \rho_0 \exp \left( - \int_0^t \text{tr}(\mathbf{A}(\mathbf{I} + s\mathbf{A})^{-1}) ds \right). \tag{A5}$$

REFERENCES

- <sup>1</sup>G. Pahlani, T. E. Schwartzentruber, and R. James, "Investigation of the breakdown of Navier-Stokes equation using objective molecular dynamics," AIAA Paper No. 2022-1012, 2022.
- <sup>2</sup>G. Pahlani, T. E. Schwartzentruber, and R. D. James, "A constitutive relation generalizing the Navier-Stokes theory to high-rate regimes," (unpublished).
- <sup>3</sup>M. D. Kroells, C. Amato, E. Torres, T. E. Schwartzentruber, and G. V. Candler, "Detailed comparison of diffusive transport phenomena between CFD and DSMC," AIAA Paper No. 2020-1229, 2020.
- <sup>4</sup>V. Garzó and A. Santos, *Kinetic Theory of Gases in Shear Flows: Nonlinear Transport* (Springer Science & Business Media, 2003), Vol. 131.
- <sup>5</sup>N. Singh and T. E. Schwartzentruber, "Nonequilibrium dissociation and recombination models for hypersonic flows," *AIAA J.* **60**, 2810–2825 (2022).
- <sup>6</sup>N. Singh and T. Schwartzentruber, "Consistent kinetic-continuum dissociation model—II: Continuum formulation and verification," *J. Chem. Phys.* **152**, 224303 (2020).
- <sup>7</sup>R. S. Chaudhry, N. Singh, M. S. Grover, T. E. Schwartzentruber, and G. V. Candler, "Implementation of a nitrogen chemical kinetics model based on ab-initio data for hypersonic CFD," AIAA Paper No. 2018-3439, 2018.
- <sup>8</sup>G. A. Bird, *Molecular Gas Dynamics and the Direct Simulation of Gas Flows* (Clarendon Press, 1994).
- <sup>9</sup>I. D. Boyd and T. E. Schwartzentruber, *Nonequilibrium Gas Dynamics and Molecular Simulation* (Cambridge University Press, 2017), Vol. 42.
- <sup>10</sup>D. Frenkel and B. Smit, *Understanding Molecular Simulation: From Algorithms to Applications* (Elsevier, 2001), Vol. 1.
- <sup>11</sup>M. P. Allen and D. J. Tildesley, *Computer Simulation of Liquids* (Oxford University Press, 2017).
- <sup>12</sup>K. Koura, "4 Carlo direct simulation of rotational relaxation of diatomic molecules using classical trajectory calculations: Nitrogen shock wave," *Phys. Fluids* **9**, 3543–3549 (1997).
- <sup>13</sup>T. E. Schwartzentruber, M. S. Grover, and P. Valentini, "Direct molecular simulation of nonequilibrium dilute gases," *J. Thermophys. Heat Transfer* **32**, 892–903 (2018).

Downloaded from http://pubs.aip.org/aip/pof/article-pdf/doi/10.1063/5.0150492/17945365/067111\_1\_5.0150492.pdf



- <sup>14</sup>E. C. Geistfeld, E. Torres, and T. E. Schwartzentruber, "Quasi classical trajectory analysis of oxygen recombination using a consistent binary lifetime framework," AIAA Paper No. 2022-1635, 2022.
- <sup>15</sup>E. Torres and T. E. Schwartzentruber, "Direct molecular simulation of nitrogen dissociation under adiabatic postshock conditions," *J. Thermophys. Heat Transfer* **34**, 801–815 (2020).
- <sup>16</sup>P. Valentini, T. E. Schwartzentruber, J. D. Bender, and G. V. Candler, "Dynamics of nitrogen dissociation from direct molecular simulation," *Phys. Rev. Fluids* **1**, 043402 (2016).
- <sup>17</sup>P. Valentini, T. E. Schwartzentruber, J. D. Bender, I. Nompelis, and G. V. Candler, "Direct molecular simulation of nitrogen dissociation based on an *ab initio* potential energy surface," *Phys. Fluids* **27**, 086102 (2015).
- <sup>18</sup>K. Dayal and R. D. James, "Nonequilibrium molecular dynamics for bulk materials and nanostructures," *J. Mech. Phys. Solids* **58**, 145–163 (2010).
- <sup>19</sup>K. Dayal and R. D. James, "Design of viscometers corresponding to a universal molecular simulation method," *J. Fluid Mech.* **691**, 461–486 (2012).
- <sup>20</sup>G. Pahlani, E. Torres, T. E. Schwartzentruber, and R. D. James, "Objective molecular dynamics of dissociating nitrogen under high temperature conditions," AIAA Paper No. 2021-0707, 2021.
- <sup>21</sup>G. Pahlani, A. R. Balakrishna, and R. D. James, "Objective molecular dynamics study of cross slip under high-rate deformation," (unpublished).
- <sup>22</sup>A. Aghaei and K. Dayal, "Symmetry-adapted non-equilibrium molecular dynamics of chiral carbon nanotubes under tensile loading," *J. Appl. Phys.* **109**, 123501 (2011).
- <sup>23</sup>R. D. James, A. Nota, and J. J. Velázquez, "Long-time asymptotics for homoeenergetic solutions of the Boltzmann equation: Collision-dominated case," *J. Nonlinear Sci.* **29**, 1943–1973 (2019).
- <sup>24</sup>R. D. James, A. Nota, and J. J. Velázquez, "Long time asymptotics for homoeenergetic solutions of the Boltzmann equation. Hyperbolic-dominated case," *Nonlinearity* **33**, 3781 (2020).
- <sup>25</sup>G. Pahlani, T. E. Schwartzentruber, and R. D. James, "Objective molecular dynamics for atomistic simulation of macroscopic fluid motion," *J. Comput. Phys.* **478**, 111938 (2023).
- <sup>26</sup>Y. Pauku, K. R. Yang, Z. Varga, and D. G. Truhlar, "Global *ab initio* ground-state potential energy surface of  $N_4$ ," *J. Chem. Phys.* **139**, 044309 (2013).
- <sup>27</sup>R. Jaffe, D. Schwenke, G. Chaban, and W. Huo, "Vibrational and rotational excitation and relaxation of nitrogen from accurate theoretical calculations," AIAA Paper No. 2008-1208, 2008.
- <sup>28</sup>M. S. Grover and P. Valentini, "*Ab initio* simulation of hypersonic flows past a cylinder based on accurate potential energy surfaces," *Phys. Fluids* **33**, 051704 (2021).
- <sup>29</sup>C. Kondur and K. A. Stephani, "Molecular recombination dynamics of nitrogen from quasi-classical trajectory simulations of the  $N_3$  system," AIAA Paper No. 2022-1906, 2022.
- <sup>30</sup>R. Jaffe, D. Schwenke, and G. Chaban, "Vibration-rotation excitation and dissociation in  $N_2$ - $N_2$  collisions from accurate theoretical calculations," AIAA Paper No. 2010-4517, 2010.
- <sup>31</sup>M. Panesi, R. L. Jaffe, D. W. Schwenke, and T. E. Magin, "Rovibrational internal energy transfer and dissociation of  $N_2(^1\Sigma_g^+)$ - $N(^4S_u)$  system in hypersonic flows," *J. Chem. Phys.* **138**, 044312 (2013).
- <sup>32</sup>M. Panesi, A. Munafò, T. Magin, and R. Jaffe, "Nonequilibrium shock-heated nitrogen flows using a rovibrational state-to-state method," *Phys. Rev. E* **90**, 013009 (2014).
- <sup>33</sup>M. Capitelli, G. Colonna, and F. Esposito, "On the coupling of vibrational relaxation with the dissociation-recombination kinetics: From dynamics to aerospace applications," *J. Phys. Chem. A* **108**, 8930–8934 (2004).
- <sup>34</sup>E. Torres, G. Bellas-Chatzigeorgis, and T. E. Magin, "How to build coarse-grain transport models consistent from the kinetic to fluid regimes," *Phys. Fluids* **33**, 036110 (2021).
- <sup>35</sup>A. C. Van Duin, S. Dasgupta, F. Lorant, and W. A. Goddard, "ReaxFF: A reactive force field for hydrocarbons," *J. Phys. Chem. A* **105**, 9396–9409 (2001).
- <sup>36</sup>N. S. Parsons, T. Zhu, D. A. Levin, and A. C. Van Duin, "Development of DSMC chemistry models for nitrogen collisions using accurate theoretical calculations," AIAA Paper No. 2014-1213, 2014.
- <sup>37</sup>N. Parsons, D. A. Levin, A. C. van Duin, and T. Zhu, "Modeling of molecular nitrogen collisions and dissociation processes for direct simulation Monte Carlo," *J. Chem. Phys.* **141**, 234307 (2014).
- <sup>38</sup>D. W. Schwenke, "Calculations of rate constants for the three-body recombination of  $H_2$  in the presence of  $H_2$ ," *J. Chem. Phys.* **89**, 2076–2091 (1988).
- <sup>39</sup>E. Torres and T. E. Schwartzentruber, "Direct molecular simulation of dissociating nitrogen in an adiabatic reactor," AIAA Paper No. 2019-1049, 2019.
- <sup>40</sup>R. Jaffe, "The calculation of high-temperature equilibrium and nonequilibrium specific heat data for  $N_2$ ,  $O_2$  and  $NO$ ," AIAA Paper No. 87-1633, 1987.
- <sup>41</sup>M. S. Grover, P. Valentini, E. Josyula, and R. S. Chaudhry, "Vibrational state-to-state and multiquantum effects for  $N_2 + N_2$  interactions at high temperatures for aerothermodynamic applications," AIAA Paper No. 2020-1227, 2020.
- <sup>42</sup>G. Colonna, L. D. Pietanza, and M. Capitelli, "Recombination-assisted nitrogen dissociation rates under nonequilibrium conditions," *J. Thermophys. Heat Transfer* **22**, 399–406 (2008).
- <sup>43</sup>P. V. Marrone and C. E. Treanor, "Chemical relaxation with preferential dissociation from excited vibrational levels," *Phys. Fluids* **6**, 1215–1221 (1963).
- <sup>44</sup>D. Bose and G. V. Candler, "Simulation of hypersonic flows using a detailed nitric oxide formation model," *Phys. Fluids* **9**, 1171–1181 (1997).
- <sup>45</sup>H. Luo, A. A. Alexeenko, and S. O. Macheret, "Assessment of classical impulsive models of dissociation in thermochemical nonequilibrium," *J. Thermophys. Heat Transfer* **32**, 861–868 (2018).
- <sup>46</sup>R. S. Chaudhry, "Modeling and analysis of chemical kinetics for hypersonic flows in air," Ph.D. thesis (University of Minnesota, 2018).
- <sup>47</sup>W. G. Vincenti, *Introduction to Physical Gas Dynamic* (Krieger Pub Co, 1975); available at <https://www.amazon.com/Introduction-Physical-Gas-Dynamics-Vinenti/dp/0882753096>.
- <sup>48</sup>R. E. Graves and B. M. Argrow, "Bulk viscosity: Past to present," *J. Thermophys. Heat Transfer* **13**, 337–342 (1999).
- <sup>49</sup>K. Xu and E. Josyula, "Continuum formulation for non-equilibrium shock structure calculation," *Commun. Comput. Phys.* **1**, 425–448 (2006); available at <https://hdl.handle.net/1783.1/2617>.
- <sup>50</sup>J. W. Streicher, A. Krish, and R. K. Hanson, "Coupled vibration-dissociation time-histories and rate measurements in shock-heated, nondilute  $O_2$  and  $O_2$ -Ar mixtures from 6000 to 14 000 K," *Phys. Fluids* **33**, 056107 (2021).
- <sup>51</sup>E. Torres and T. E. Schwartzentruber, "Direct molecular simulation of oxygen dissociation across normal shocks," *Theor. Comput. Fluid Dyn.* **36**, 41–80 (2022).
- <sup>52</sup>G. Colonna, I. Armenise, D. Bruno, and M. Capitelli, "Reduction of state-to-state kinetics to macroscopic models in hypersonic flows," *J. Thermophys. Heat Transfer* **20**, 477–486 (2006).
- <sup>53</sup>E. Plönjes, P. Palm, W. Lee, M. D. Chidley, I. V. Adamovich, W. R. Lempert, and J. W. Rich, "Vibrational energy storage in high pressure mixtures of diatomic molecules," *Chem. Phys.* **260**, 353–366 (2000).
- <sup>54</sup>E. Kustova, E. Nagnibeda, T. Y. Alexandrova, and A. Chikhaoui, "On the non-equilibrium kinetics and heat transfer in nozzle flows," *Chem. Phys.* **276**, 139–154 (2002).
- <sup>55</sup>G. Colonna, M. Tuttafesta, M. Capitelli, and D. Giordano, "Non-Arrhenius  $NO$  formation rate in one-dimensional nozzle airflow," *J. Thermophys. Heat Transfer* **13**, 372–375 (1999).
- <sup>56</sup>G. V. Candler, "Rate effects in hypersonic flows," *Annu. Rev. Fluid Mech.* **51**, 379–402 (2019).
- <sup>57</sup>I. Nompelis, *Computational Study of Hypersonic Double-Cone Experiments for Code Validation* (University of Minnesota, 2004).